Article

A reaction kinetic model for 2, 4-D decomposition in aqueous media including direct photolysis, direct ozonation, UVC and pH enhancement

Maria Belen Gilliard, Carlos Martín, Alberto Cassano, and María Eugenia Lovato

Ind. Eng. Chem. Res., **Just Accepted Manuscript** • DOI: 10.1021/ie400957m • Publication Date (Web): 03 Sep 2013

A reaction kinetic model for 2,4-D decomposition in aqueous media including direct photolysis, direct ozonation, UVC and pH enhancement

María B. Gilliard[1], Carlos A. Martín[1,2], Alberto E. Cassano[1,2], María E. Lovato[1]*

(1) INTEC (Instituto de Desarrollo Tecnológico para la Industria Química). Universidad Nacional del Litoral and CONICET. Santa Fe. Argentina. Tel - Fax: + 54 (0)342 4511087

(2) Facultad de Ingeniería y Ciencias Hídricas. Ciudad Universitaria. Paraje El Pozo. Santa Fe, Argentina

* e-mail: mlovato@santafe-conicet.gov.ar

ABSTRACT

This report presents a comprehensive study of the degradation kinetics of herbicide 2,4-D using ozone with and without intensification with UVC radiation. The by-products cause several series-parallel reactions that compete with the process of photon absorption when radiation is applied.

Five processes were analyzed separately: (i) the direct photolysis of 2,4-D and its main by-products, (ii) direct ozonation in the absence of hydroxyl radicals using tert-butanol as radical scavenger, (iii) the oxidation when ozone reacts in parallel with hydroxyl radicals, (iv) the reaction enhanced with UVC radiation and (v) the oxidation improved by pH modifications.

A kinetic model was developed based on the main reaction by-products. The corresponding parameters of the reacting system were determined (9 of its 29 kinetic constants were previously unknown).

Simulation results, including a rigorous description of the reacting system and the radiation field (having dark and illuminated volumes) agree very well with the experimental data.

KEYWORDS

Ozone, 2,4-Dichlorophenoxyacetic acid, UVC radiation, Reactor-reaction modeling

1. INTRODUCTION

Concern for the release of pesticides and their impact on the environment has led to the prohibited use of several chemical groups such as organochlorinated (e.g., Aldrin, Dieldrin, Chlordane, DDT, Heptachlor) as well as organophosphorated (e.g., Parathion)[1] compounds. However, in the case of other products such as chlorophenoxyacetic herbicides, classified as moderately toxic by the World Health Organization, their application remains widespread[2-6]. These herbicides, whose most commonly used exponent is the 2,4 dichlorophenoxyacetic acid (2,4-D), are characterized as being slowly degradable via microbiological processes[7-9] and by generating stable by-products, which not always have lower toxicity. Because herbicides and pesticides exhibit some degree of water solubility, much of the contamination of natural waterways is released from agricultural field runoffs, which are considered to be nonpoint type sources of pollution[7]. Therefore, development of efficient degradation processes for these compounds is important. Among them, those that are known as Advanced Oxidation Processes (AOPs) have proved to be capable of completely degrading many different families of compounds, transforming them into water, carbon dioxide and inorganic acids or salts.

Different authors have studied the degradation of 2,4-D using AOPs, such as Fenton, photo-Fenton and electro-Fenton[10-12], photocatalysis[4,13-16], H_2O_2/UV[17-18], anodic oxidation[19], sonolysis[20], radiolysis[21-23]; O_3, O_3/H_2O_2, O_3 plus catalyst[24-33] to quote only a few examples. These studies include kinetic analyses, proposals of reaction schemes, intermediates identification, determination of different efficiencies and yields, etc.

Although all AOPs have in common the participation of hydroxyl radicals as non-selective oxidizing agents, they differ in the mechanisms through which these radicals are generated. In some cases, other compounds capable of directly reacting with pollutants are also involved,

giving rise to parallel paths of reaction (e.g., direct ozonation, UV photolysis). The combined removal alternatives can be more efficient for treating molecules refractory to degradation since different reaction pathways are initiated, involving selective and non-selective attacks, as it is the case where simultaneous molecular ozone and radicals formed from ozone dissolution in water may operate simultaneously[26,34-36]. Moreover, they may also be strongly enhanced by the inclusion of UV radiation[26] or even changing the pH[10,24-25,29-30].

The study of the potential "oxidation/mineralization" of a complex system such as the one originated in the oxidation of 2,4-D using O_3/UVC represents an interesting challenge since special difficulties arise in the process under consideration. In fact, when the reaction proceeds, the system becomes a multicomponent mixture with competitive reactions in series and parallel paths, such as the photolysis of reagents and intermediates, selective oxidation reactions produced directly by molecular ozone and indirect reactions where hydroxyl radicals take part in a non selective degradation of reagents and intermediates. Concomitantly, the modeling of the reactor needs the resolution of the mass and radiant energy balances, which, considering the characteristics of the reactor employed, include "dark" and "irradiated" volumes[36], and a variable spatial distribution of radiant energy which is also a function of time[37].

Hence, this work studies the kinetics of the degradation of 2,4-D isolating all possible reaction paths and taking into account the increase in the reaction rate by the presence of a non uniform radiation field or the effects produced by changing the pH of the medium. In addition the modeling of the reacting system in a comprehensive and rigorous way which, when radiation is applied, includes dark and illuminated volumes, was made.

Since at this stage of our study the first objective is to obtain intrinsic kinetic constants, this part of the work was done using pure water in order to avoid contaminating the results with interferences produced by other compounds present in natural waters. Then, having this

information, it will be possible to study the effects and changes that will be produced on these undisguised kinetic values by the incorporation of impurities existing in systems more representative of realistic compositions of contaminated waters which, ultimately, constitute the final target of every applied orientated work.

2. MATERIALS AND METHODS

2.1 Materials

Reagents were used as purchased. 2,4-D (>99%), 2,4-Dichlorophenol (2,4-DCP, >99%), 2-Chlorohydroquinone (2-CHQ, >85%) and Indigo Potassium Trisulfonate (> 99%) were supplied by Aldrich. Oxygen (>95%) was provided by Air Liquide Argentina. Methanol (>99.5%) and tert-butanol (t-BuOH, >99.5%) were purchased from Sintorgan. Sodium Phosphate Monobasic (> 99%) and Sodium Phosphate Dibasic Heptahydrated (> 98%) were supplied by Anhedra and Cicarelli, respectively. Potassium Chloride (> 99%) was provided by Merck.

2.2 The reactor configuration

All degradation experiments were conducted in the recirculation system depicted in Figure 1. Ozone was produced from pure O_2. The temperature of the system was kept constant at 20 ±0.1 °C. The reactor could be operated in the dark or could be irradiated by means of two low pressure Hg germicidal lamps. The corresponding emission spectra and additional details of the lamps and reacting system can be found in the Supporting Information.

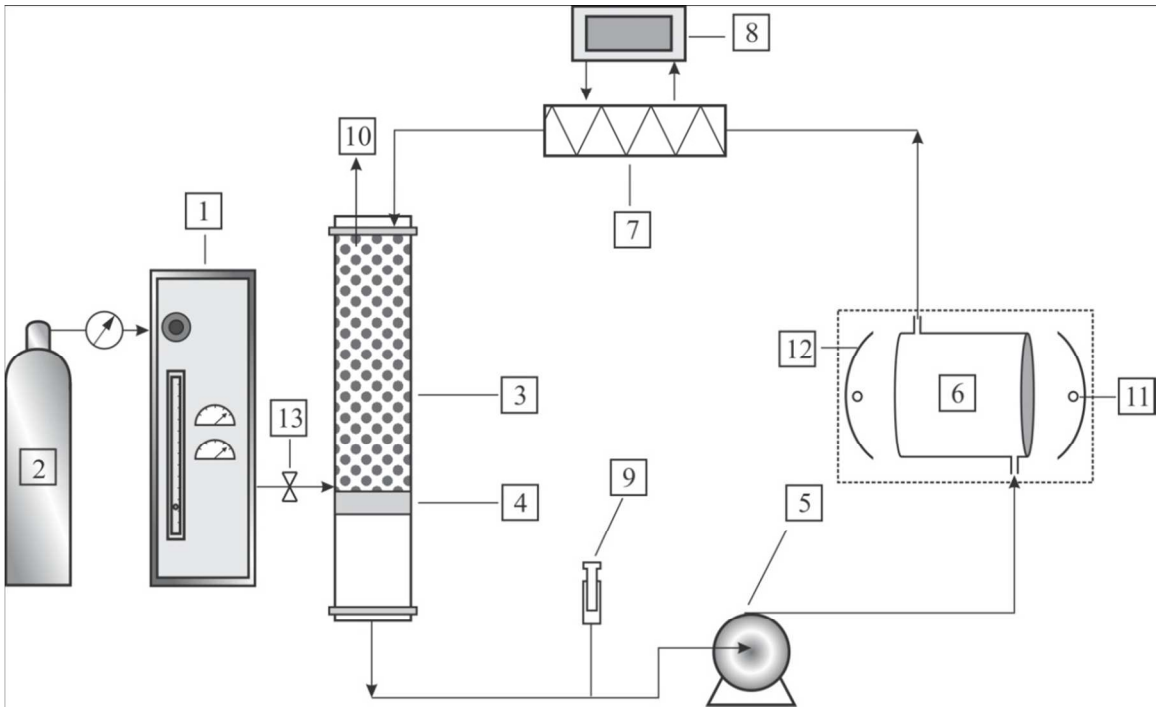

Figure 1. Reactor configuration. (1) Ozone generator. (2) O_2 cylinder. (3) Absorption column. (4) Perforated plate. (5) Centrifugal pump. (6) Photoreactor. (7) Heat exchanger. (8) Thermostatic bath. (9) Sampling port. (10) Venting outlet. (11) Germicidal lamps. (12) Parabolic reflectors. (13) Intake valve

2.3 Experimental procedure

The oxygen supply to the ozone generator was turned on and the produced mixture of O_3/O_2 was vented while the germicidal lamps were turned on (during this time the shutters at the reactor windows were on). The solution was prepared at the desired concentration of 2,4-D, and began to recirculate by means of the centrifugal pump through the system to achieve good mixing. This stabilization was carried out at least for 30 min before starting each experiment. The moment at which the intake valve of the absorption column was open and the shutters were removed (in runs involving UVC) was considered the initial time. From this moment on, samples were taken at definite time intervals and the concentrations of 2,4-D, 2,4-DCP, 2-CHQ and chloride ion (Cl^-), as well as the values of Total Organic Carbon (TOC) and pH were measured.

The pH of the solution was the natural one produced by the dissolution of 2,4-D in water. Depending upon the initial concentration of 2,4-D, the value varied from 2.5 to 3.0 ± 0.1 at the beginning of the reaction to 2.0 to 2.5 ± 0.1 at the end, due to the formation of aliphatic acids and HCl. To study the effect of pH under controlled conditions, in order to maintain the invariance of the adopted values (7 and 10) preventing its rapid evolution to acidic conditions (pH ≈ 2.5 to 3) typical buffer solutions $\left(NaH_2PO_4 / Na_2HPO_4\right)$ were added to the medium.

According to indisputable literature data[7,12,21,28,38], most of 2,4-D degradation passes through 2,4-DCP in a first step; therefore, it was considered pertinent to start some runs from 2,4-DCP directly to unravel several aspects of the degradation intermediates of 2,4-D oxidation. Hence, additional runs were made degrading this compound directly.

An equivalent set of experiments was carried out in the presence of t-BuOH as •OH radical scavenger[39]. A molar relationship of t-BuOH with respect to O_3 equal to 1 was utilized, which is considered sufficient for the radical-mediated mechanism inhibition[32].

Additional details can be found in the Supporting Information.

2.4. Analyses

The concentrations of 2,4-D and its stable aromatic intermediates 2,4-DCP and 2-CHQ were followed using HPLC. In order to measure Cl^- concentration and assist in the identification of glycolic and oxalic acid, ion chromatography was applied. In both techniques, injections were performed in triplicate for each sample.

The oxidation intermediates and degradation products of 2,4-D by the ozone process (including those for which it was not possible to follow their quantitative evolution because further oxidation proceeded too rapidly) were identified using chemical derivatization and GC-MS analysis[40].

The mineralization of herbicide solutions was monitored for their TOC decay, using a TOC analyzer. Residual ozone in the aqueous phase was measured using the Indigo Method[41]. pH was monitored along the reaction using a digital thermo-pH-meter. The concentration of t-BuOH was analyzed using a gas chromatograph (GC) equipped with a flame ionization detector (FID). In all cases, the concentration of t-BuOH was almost constant, which confirms that the selected molar relationship was correct.

The local values of the incident radiation were calculated with a radiation model as described in the following section. For this purpose, it was necessary to know the value of this variable in the inner side of the reactor wall. It was obtained experimentally resorting to precise actinometric measurements using potassium ferrioxalate[42], interpreting the data according to the method proposed by Zalazar et al.[43]. This method provides more accurate results than an experimental measurement of the radiation fluxes at any point inside or outside the reactor.

Additional details and results can be found in the Supporting Information.

3. MODELING OF THE REACTOR AND THE RADIATION FIELD

3.1. The reactor mass balance

For the liquid phase, the adopted experimental device is an isothermal, well-stirred batch recycling reactor. The operating conditions in the system may be summarized as follows: (i) the reactor volume is smaller than the total volume, $V_R/V_{Tot} < 1$ (and even better if it is <<1), (ii) there is perfect mixing in the whole recycling system, (iii) high recirculating flow rate is applied, and (iv) isothermal operation is maintained throughout. As shown in the Supporting Information, for runs without irradiation or if the whole reacting system (V_{Tot}) were irradiated, a rigorous mass balance for this reactor yields:

$$\left.\frac{dC_i(t)}{dt}\right|_{Sampling} = \left[R_{i,\,Dark}\left(\underline{x},t\right)\right]_{V_{Tot.}} \tag{1.a}$$

$$\left.\frac{dC_i(t)}{dt}\right|_{Sampling} = \left[R_{i,\,Dark}\left(\underline{x},t\right) + R_{i,\,Irr.}\left(\underline{x},t\right)\right]_{V_{Tot.}} \tag{1.b}$$

$i = 1, 2, ...n$

And for the operation of the system when only V_R is irradiated, the mass balance is:

$$\left.\frac{dC_i(t)}{dt}\right|_{Sampling} = \left\langle R_{i,\,Dark}\left(\underline{x},t\right)\right\rangle_{V_{Tot.}} + \left(\frac{V_R}{V_{Tot}}\right)\left\langle R_{i,\,Irr.}\left(\underline{x},t\right)\right\rangle_{V_R} \tag{1.c}$$

$i = 1, 2, ...n$

From the condition of very good mixing operation, all concentrations are constant in space. Consequently, the only variable that must be averaged is the local volumetric rate of photon absorption (LVRPA) that participates in the initiation steps. The value of the LVRPA must be obtained from a photon balance.

3.2. The radiation model

As shown in the Supporting Information, a one-dimensional radiation model can be used for the employed lamp-reflector-reactor system. With lamps with monochromatic emission (λ=253.7 nm) and the reactor irradiated from both sides, the following expression results for the absorbed radiation:

$$\left\langle e_i^a(t)\right\rangle_{L_R} = \frac{2\,\kappa_i(t)\,G_{W(I-II)}}{\sum_j \kappa_j(t)\,L_R}\left\{1-\exp\left[-\left(\sum_j \kappa_j(t)\right)L_R\right]\right\} \tag{2}$$

3.3. The boundary condition

In Eq. (2), G_W represents the incident radiation at the reactor wall. As indicated in Section 2.4, both values, $G_{W,I}$ and $G_{W,II}$, were obtained from actinometer measurements[42-43].

The results for the two different irradiating conditions employed in this study (lamps of 15 W and 40 W) are: $G_W = 2.14 \times 10^{-8}$ and 4.81×10^{-8} Einstein cm^{-2} s^{-1}, respectively.

4. A REACTION SCHEME

The complete mechanism of the reaction of 2,4-D decomposition is undoubtedly very complex and quite possibly, still not fully known as of today. Numerous species were found in the decomposition of 2,4-D employing several AOPs, with and without the presence of UVC radiation. Many of the known intermediates were not possible to quantify in our experimental analyses, possibly because their oxidation proceeds very fast. Others were detected at trace levels and identified after a process of derivatization and ulterior analysis by GC-MS. Finally, others were known to have been found by other authors, but not in our case. The pertinent data can be found in the Supporting Information (Table S.1).

In what follows, a summary of the species that can be found in this reaction are listed, providing a brief indication of the corresponding concentration levels encountered in our work and, in all cases, literature references that support our list. Some of them correspond to runs where ter-butanol (used as a hydroxyl radical scavenger) was present.

Table 1. Chemical species that are present in the decomposition of 2,4-D

Measured in this work	
Chemical Species	**Selected references**
2,4-D, ozone, t-BuOH, 2,4-DCP, 2-CHQ, glycolic acid, oxalic acid	5, 7, 12, 20-21, 24, 26, 28, 30, 38, 44-48
Detected traces and ulterior characterization by mass spectroscopy	
Chemical Species	**Selected references**
4,6-dichlororesorcinol, 3,5-dichlorocatechol, maleic	12, 28, 30, 39, 44-45, 48-49

acid, fumaric acid, 2,3-dihydroxysuccinic acid, tartaric acid, propanedioic acid, 2-dydroxypropan-edioic acid	
Detected by other authors	
Chemical species	**Selected references**
2,4-Dichlororesorcinol, 2- chlorobenzoquinone, 4-chlo-rocatechol, hydroquinone, 2-chloro-4-hydro-xyphenoxyacetic acid, 4-chloro-2-hydroxyphe-noxyacetic acid, glyoxylic acid, 3-hydroxy-2,4-Dichlorophenoxyacetic acid, 5-hydroxy-2,4-Dichloro-phenoxyacetic acid, 6-hydroxy-2,4-Dichlorophenoxyacetic acid. formic acid, acetic acid, glycerol, maleic anhydride, lactic acid, pyruvic acid	5, 12, 21, 28, 30, 38, 44-45, 48-49

For practical purposes, in order to carry out the design of a reactor for 2,4-D elimination, it is not essential to have a complete kinetic model that could provide all the parameters of a large set of mechanistic steps, not fully well established yet. After all, as stated by Boudart and Djega-Mariadassou[50], "reaction mechanisms come and go and their ephemeral existence is often disconcerting. By contrast, the results of good chemical kinetics remain unchanged, whatever the future revisions of the underlying mechanism". Even if not the best of all starting points, what is really needed for practical purposes is a good description of the progress of the reaction. On this basis, in this work we tried to build a kinetic model that includes only some of the major products of the reaction: especially the *aromatic* ones that are found with significant concentrations. (See Table 1). This result should be accompanied by an assessment of the TOC evaluation to verify complete mineralization. This reasoning is even more valid because the results of the analysis of the final TOC can be compared with the production of chloride ions that are very easy to measure and observe the closure of a mass balance. This parity plot would ensure the total disappearance

of all chlorinated organic species that constitute chemical species that almost always have some degree of toxicity and must be undoubtedly eliminated.

In conclusion, proposing a complete mechanism including all the compounds listed in Table 1 is not the purpose of this work. As a result, the kinetic model will be based on the well known parameters of the decomposition of ozone and the detailed monitoring of ozone concentrations, 2,4-D, 2,4-DCP, 2-CHQ, chloride ion and TOC. The search for unknown parameters in this report will always be related to this intention of arriving at a useful but simplified reaction scheme.

However, even under these limitations, a good kinetic study of this reaction is not a simple exercise. It involves: (i) Direct photolysis, (ii) Direct ozonation in the absence of •OH radicals resorting to the presence of a radical scavenger, (iii) Direct ozonation under the existence of the normal •OH radicals at equilibrium concentrations, (iv) Enhanced ozonation by the presence of UVC radiation and (v) Improving the reaction efficacy by raising the pH to neutral and alkaline conditions. Figure 2 depicts the conceptual reaction scheme developed along this work. The change of pH was not included in the figure because it involves only a variation in the operating conditions.

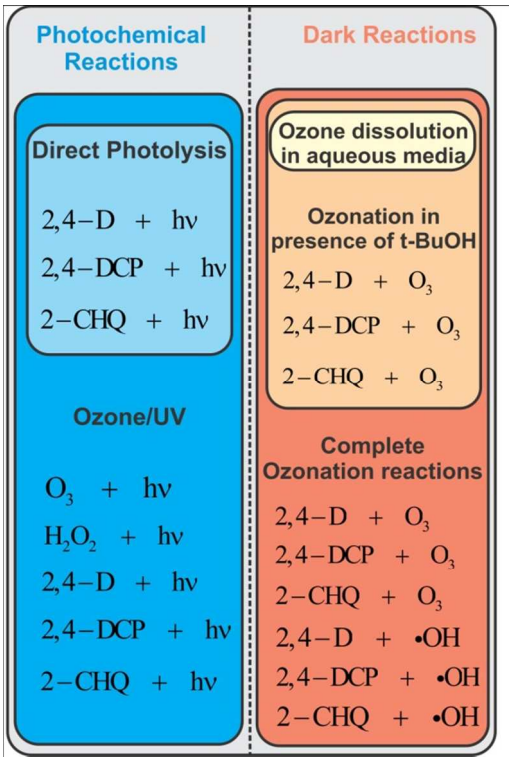

Figure 2. Conceptual reaction scheme

5. THE KINETIC MODEL

5.1. Direct photolysis

A series of experiments were made to evaluate direct photolysis of 2,4-D. The initial concentrations of 2,4-D were 2.2 $\times 10^{-7}$ and 1.37 $\times 10^{-7}$ mol cm^{-3} (50 and 30 ppm), and the incident radiation at the reactor wall was 4.81 $\times 10^{-8}$ Einstein cm^{-2} s^{-1} (corresponding to the 40 W lamps). The molar linear absorption coefficients of 2,4-D, 2,4-DCP and 2-CHQ are 4.09 $\times 10^{5}$, 4.64 $\times 10^{5}$ and 6.08 $\times 10^{5}$ cm^{2} mol^{-1}, respectively (Napierian values, experimentally measured and compared with the values published by Alfano et al.[17]).

5.1.1 Analysis and interpretation of the results

The following reaction scheme is proposed for the photolysis of 2,4-D, 2,4-DCP and 2-CHQ:

$$2,4\text{–D} \xrightarrow{h\nu} 2,4\text{–DCP} + \text{Prod}_1 \; ; \qquad \phi_{2,4\text{–D}} \tag{A}$$

$$2,4-\text{DCP} \xrightarrow{h\nu} 2-\text{CHQ} + \text{Prod}_2 \; ; \qquad \phi_{2,4-\text{DCP}} \tag{B}$$

$$2-\text{CHQ} \xrightarrow{h\nu} \text{Prod}_3 \; ; \qquad \phi_{2-\text{CHQ}} \tag{C}$$

The corresponding reaction rates for these irradiated elementary steps are:

$$R_{(\text{Irr.},2,4\text{–D})} = -\phi_{(2,4\text{–D})}\, e^{a}_{(2,4\text{–D})} \tag{3}$$

$$R_{(\text{Irr.},2,4\text{–DCP})} = \phi_{(2,4\text{–D})}\, e^{a}_{(2,4\text{–D})} - \phi_{(2,4\text{–DCP})}\, e^{a}_{(2,4\text{–DCP})} \tag{4}$$

$$R_{(\text{Irr.},2\text{–CHQ})} = \phi_{(2,4\text{–DCP})}\, e^{a}_{(2,4\text{–DCP})} - \phi_{(2\text{–CHQ})}\, e^{a}_{(2\text{–CHQ})} \tag{5}$$

These reactions take place in the irradiated reactor exclusively, thus:

$$\left.\frac{dC_{2,4\text{–D}}(t)}{dt}\right|_{\text{Sampling}} = \frac{V_R}{V_{\text{Tot}}}\left\langle R_{\text{Irr.},2,4\text{–D}}(t)\right\rangle_{V_R} \tag{6}$$

$$\left.\frac{dC_{2,4\text{–DCP}}(t)}{dt}\right|_{\text{Sampling}} = \frac{V_R}{V_{\text{Tot}}}\left\langle R_{\text{Irr.},2,4\text{–DCP}}(t)\right\rangle_{V_R} \tag{7}$$

$$\left.\frac{dC_{2\text{–CHQ}}(t)}{dt}\right|_{\text{Sampling}} = \frac{V_R}{V_{\text{Tot}}}\left\langle R_{\text{Irr.},2\text{–CHQ}}(t)\right\rangle_{V_R} \tag{8}$$

To incorporate Eqs. (3), (4) and (5) into Eqs. (6), (7) and (8), we need the respective averaged values of the LVRPA:

$$\left\langle e^{a}_{2,4\text{–D}}(t)\right\rangle_{L_R} = \frac{2\,\kappa_{2,4\text{–D}}(t)\,G_{\text{W(I–II)}}}{\left(\kappa_{2,4\text{–D}} + \kappa_{2,4\text{–DCP}} + \kappa_{2\text{–CHQ}}\right)L_R} \times \left\{1 - \exp\left[-\left(\kappa_{2,4\text{–D}} + \kappa_{2,4\text{–DCP}} + \kappa_{2\text{–CHQ}}\right)L_R\right]\right\} \tag{9}$$

$$\left\langle e^{a}_{2,4-DCP}(t)\right\rangle_{L_R} = \frac{2\,\kappa_{2,4-DCP}(t)\,G_{W(I-II)}}{\left(\kappa_{2,4-D}+\kappa_{2,4-DCP}+\kappa_{2-CHQ}\right)L_R}\times \left\{1-\exp\left[-\left(\kappa_{2,4-D}+\kappa_{2,4-DCP}+\kappa_{2-CHQ}\right)L_R\right]\right\} \quad (10)$$

$$\left\langle e^{a}_{2-CHQ}(t)\right\rangle_{L_R} = \frac{2\,\kappa_{2-CHQ}(t)\,G_{W(I-II)}}{\left(\kappa_{2,4-D}+\kappa_{2,4-DCP}+\kappa_{2-CHQ}\right)L_R}\times \left\{1-\exp\left[-\left(\kappa_{2,4-D}+\kappa_{2,4-DCP}+\kappa_{2-CHQ}\right)L_R\right]\right\} \quad (11)$$

Once it is done, the result can be directly replaced into Eqs. (6), (7) and (8). This operation originates a system of three ordinary differential equations where the concentrations of 2,4-D, 2,4-DCP and 2-CHQ are the independent variables and the quantum yields are the unknown kinetic constants. This system of differential equations can be solved jointly with a nonlinear parameter estimator, which optimizes, at each time, the result of comparing the calculated values of concentrations with those obtained along the experimental runs. In this way, each of the unknown quantum yields can be calculated. The obtained quantum yields are: $\phi_{2,4\text{-D}} = 0.016$ mol Einstein^{-1}, $\phi_{2,4\text{-DCP}} = 0.017$ mol Einstein^{-1} and $\phi_{2\text{-CHQ}} = 0.041$ mol Einstein^{-1}.

These yields are small, which is a quantitative indication that the direct photolysis of these compounds is not very important. Still, the values of the ones corresponding to reactions (A) and (B) are very different from the one associated with reaction (C). It is interesting to note that there are values in the literature to compare with those obtained in this work. The decomposition of 2,4-D employing hydrogen peroxide was studied by Alfano et al.[17] They found the following values: $\phi_{2,4\text{-D}} = 0.0131$ mol Einstein^{-1}, $\phi_{2,4\text{-DCP}} = 0.0184$ mol Einstein^{-1} and $\phi_{2\text{-CHQ}} = 0.0426$ mol Einstein^{-1}. The agreement between the respective values is acceptable, especially considering that these authors have worked with a slightly different reaction scheme. Figure 3 shows the quality of the parameter estimation obtained.

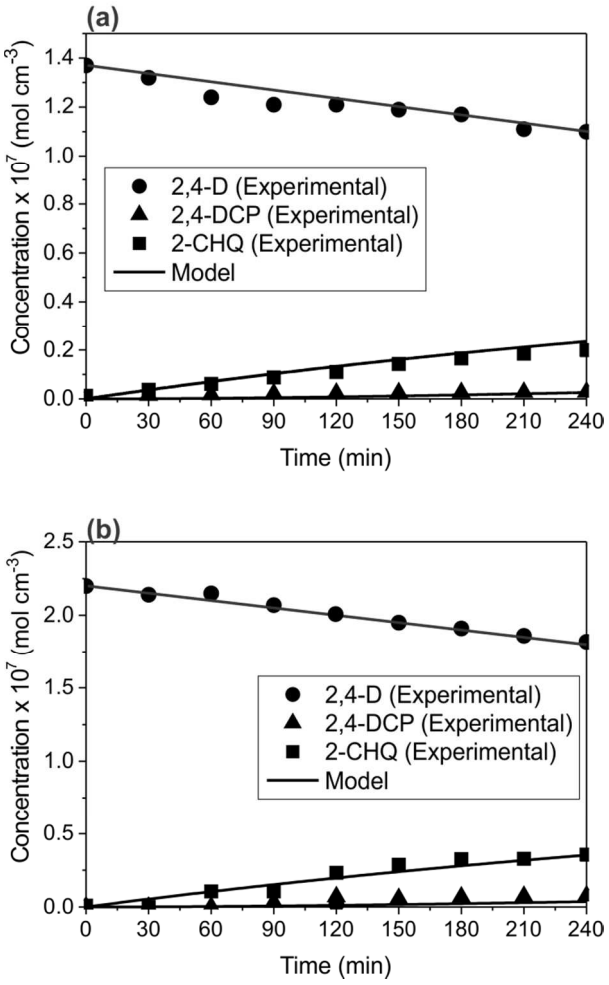

Figure 3. Direct photolysis. (a) $C^0_{2,4-D}$=1.37 × 10^{-7} mol cm^{-3} (30 ppm) and (b) $C^0_{2,4-D}$=2.20 × 10^{-7} mol cm^{-3} (50 ppm). Symbols correspond to experimental data. Solid lines correspond to simulation results obtained from the model.

5.2. Direct ozonation

The ozone concentration in the system is constant. This condition is ensured with the employed apparatus that includes a regulated, continuous feed and a very gentle ozone output stream through a venting hole. In every reaction in which ozone participates, the recycling system is a well-stirred, semi-batch reactor. The ozone consumed in all the reaction steps in which it intervenes must be replenished to keep its concentration constant, which is the proposed

operating condition of this work. For all the other species, the recycling system is a well-mixed batch reactor.

The exact value of the ozone concentration was experimentally verified for each run. The absence of pollutant or reaction products stripping was confirmed by specific tests with blank runs.

According to von Gunten[51], it can also be assumed that hydroxyl radical concentrations at each ozone concentration are also maintained constant during the experiments. This type of hypothesis is very often successfully employed when the micro steady state approximation is applied in conventional kinetic studies. Its validity is supported by the existing very low •OH radical concentrations. In addition, this estimate is even more persuasively grounded when the O_3 loading is kept constant. Under these conditions, a simplified monitoring of the reaction can be determined after the steady state concentrations of ozone are reached $\left([O_3]_{s.s.}\right)$ which in this case are 9.71×10^{-8}, 1.21×10^{-7} and 3.01×10^{-7} mol cm^{-3}, respectively (nominal values, accurately measured specifically for each case). At $[O_3]_{s.s.}$ the resistance of the ozone mass transfer from the gas phase to the liquid phase becomes negligible as the concentration of ozone is uniform throughout the liquid[34,52]. In this case, the ozone consumption rate is solely determined by the rate of chemical consumption in the bulk and equal to the instantaneous reposition by the absorption column.

The reactions between 2,4-D, 2,4-DCP and 2-CHQ with ozone are:

$$2,4-D + O_3 \rightarrow 2.4-DCP + Prod_4 \quad (D)$$

$$2,4-DCP + O_3 \rightarrow 2-CHQ + Prod_5 \quad (E)$$

$$2-CHQ + O_3 \rightarrow Prod_6 \quad (F)$$

The corresponding reaction rates are:

$$R_{2,4-D} = -k_D^* \, C_{2.4-D} \, C_{O_3} \quad (12)$$

$$R_{2,4-DCP} = k_D^* \, C_{2.4-D} \, C_{O_3} - k_E^* \, C_{2.4-DCP} \, C_{O_3} \quad (13)$$

$$R_{2-CHQ} = k_E^* \, C_{2.4-DCP} \, C_{O_3} - k_F^* \, C_{2-CHQ} \, C_{O_3} \quad (14)$$

As ozone overall oxidation occurs through a combination of molecular ozone and hydroxyl free radical pathways, the decay rate of 2,4-D for example, can be established by Eq. (15) where k_{O_3} and $k_{\cdot OH}$ are the respective reaction rate constants.

$$-\frac{d\,C_{2,4-D}}{dt} = k_{O_3} \, C_{O_3} C_{2.4-D} + k_{\cdot OH} \, C_{\cdot OH} C_{2.4-D} \quad (15)$$

To determine the nature of ozone attacks and the influence of hydroxyl radicals on ozone activity, two sets of experiments were made: (i) conventional ozonation and (ii) the same ozonation experiments in the presence of t-BuOH as radical scavenger, where only the reactions involving molecular ozone attack are present. In this way, it is possible to complete a kinetic study of this reaction. Moreover, the differentiation of the effect of ozone on the occasion that acts alone and when it does so in the presence of UVC radiation will be much more complete. On the other hand, the differentiation of both kinetic constants is very important to analyze if its value remains constant or varies when the rate of hydroxyl radical generation is altered by the inclusion of UVC radiation or the pH is changed into a definitely alkaline operating condition.

5.2.1. Direct ozonation in the presence of tert-butanol

5.2.1.1. Experiments and data

After the steady state concentrations of ozone are reached $\left([O_3]_{s.s.}\right)$, the corresponding values are: 4.5×10^{-8}, 1.2×10^{-7} and 3.18×10^{-7} mol cm^{-3}, respectively (nominal values, accurately measured specifically for each case). 2,4-D initial concentrations were 1.57×10^{-6}, 1.33×10^{-6}

and 1.57×10^{-6} mol cm^{-3}, respectively. The concentration of t-BuOH was 3.01×10^{-7} mol cm^{-3} (Value slightly greater than others reported in the literature[34,53]).

5.2.1.2. Reaction scheme and interpretation of the results

The first attention must be addressed to verify the efficiency of t-BuOH to eliminate the hydroxyl radicals. Thus, it will be possible to decide whether or not their inclusion in the reaction scheme adopted for modeling the ozonation of 2,4-D is necessary when the process is conducted in the presence of the scavenger. Consequently, the reaction that involves the interaction between the hydroxyl radical (generated in the decomposition of ozone in water) and t-BuOH will be analyzed first. The mechanism and the kinetic parameters corresponding to ozone decomposition in aqueous media are known in agreement with the information published by Lovato et al.[34]

$$t-BuOH + O_3 \rightarrow Prod_{t-BuOH,1} \quad (G)$$

$$t\text{-}BuOH + {}^{\bullet}OH \rightarrow Prod_{t-BuOH,2} \quad (H)$$

The kinetic scheme results:

Table 2. Reaction mechanism for ozone decomposition in the presence of t-BuOH

Step	Reaction	Kinetic constant – units	Reference
(1)	$O_3 + OH^- \rightarrow HO_2^- + O_2$	$k_1 = 1.7 \times 10^5$ cm^3 mol^{-1} s^{-1}	54
(2)	$O_3 + HO_2^- \rightarrow HO_2^{\bullet} + O_3^{\bullet-}$	$k_2 = 2.2 \times 10^9$ cm^3 mol^{-1} s^{-1}	55
(3)	$HO_2^{\bullet} \rightarrow O_2^{\bullet-} + H^+$	$k_3 = 7.9 \times 10^5$ s^{-1}	56
(4)	$O_2^{\bullet-} + H^+ \rightarrow HO_2^{\bullet}$	$k_4 = 5 \times 10^{13}$ cm^3 mol^{-1} s^{-1}	56
(5)	$O_3 + O_2^{\bullet-} \rightarrow O_3^{\bullet-} + O_2$	$k_5 = (1.6 \pm 0.2) \times 10^{12}$ cm^3 mol^{-1} s^{-1}	57
(6)	$O_3^{\bullet-} + H^+ \rightarrow HO_3^{\bullet}$	$k_6 = 5 \times 10^{13}$ cm^3 mol^{-1} s^{-1}	58
(7)	$HO_3^{\bullet} \rightarrow O_3^{\bullet-} + H^+$	$k_7 = 3.3 \times 10^2$ s^{-1}	58
(8)	$HO_3^{\bullet} \rightarrow {}^{\bullet}OH + O_2$	$k_8 = 1.1 \times 10^5$ cm^3 mol^{-1} s^{-1}	58

(9)	$O_3 + \bullet OH \rightarrow HO_2^{\bullet} + O_2$	$k_9 = 1.1 \times 10^{11}$ cm^3 mol^{-1} s^{-1}	59
(10)	$O_2^{\bullet -} + \bullet OH \rightarrow OH^- + O_2$	$k_{10} = (2.8 \pm 0.3) \times 10^7$ cm^3 mol^{-1} s^{-1}	60
(11)	$HO_2^- + H^+ \rightarrow H_2O_2$	$k_{11} = 5 \times 10^{13}$ cm^3 mol^{-1} s^{-1}	56
(12)	$H_2O_2 \rightarrow HO_2^- + H^+$	$k_{12} = 0.125$ s^{-1}	56
(13)	$HO_2^{\bullet} + \bullet OH \rightarrow H_2O + O_2$	$k_{13} = 5 \times 10^{12}$ cm^3 mol^{-1} s^{-1}	60
(14)	$\bullet OH + HO_3^{\bullet} \rightarrow H_2O_2 + O_2$	$k_{14} = 5 \times 10^{12}$ cm^3 mol^{-1} s^{-1}	60
(15)	$\bullet OH + H_2O_2 \rightarrow HO_2^{\bullet} + H_2O$	$k_{15} = 2.7 \times 10^{10}$ cm^3 mol^{-1} s^{-1}	61
(16)	$\bullet OH + HO_2^- \rightarrow HO_2^{\bullet} + OH^-$	$k_{16} = 7.5 \times 10^{12}$ cm^3 mol^{-1} s^{-1}	61
(17)	$\bullet OH + \bullet OH \rightarrow H_2O_2$	$k_{17} = 5.2 \times 10^{12}$ cm^3 mol^{-1} s^{-1}	62
(18)	$HO_2^{\bullet} + HO_2^{\bullet} \rightarrow H_2O_2 + O_2$	$k_{18} = 8.3 \times 10^8$ cm^3 mol^{-1} s^{-1}	63
(19)	$\text{t-BuOH} + O_3 \rightarrow \text{Prod}_{t-BuOH,1}$	$k_{19} = 3 \times 10^2$ cm^3 mol^{-1} s^{-1}	39
(20)	$\text{t-BuOH} + \bullet OH \rightarrow \text{Prod}_{t-BuOH,2}$	$k_{20} = 5 \times 10^{11}$ cm^3 mol^{-1} s^{-1}	39

The mass balance is a simple set of ordinary differential equations, for a well-stirred, isothermal, batch reactor. The reaction kinetics was formulated in terms of the mass action law for all the necessary reaction steps. In what follows, the procedure is illustrated with the mechanism proposed in Table 2 for the •OH radical. Then, it becomes necessary to resort to the solution of a system of 12 ordinary differential equations (ODE), for the reactant species present in the system. The following assumptions were made to solve the set of ODE:

(i) Taking into account that the action of the t-BuOH on ozone, as compared to the one that exercises on the •OH radicals is practically negligible in spite of the differences in their corresponding reaction rate constants, the ozone concentration in the system is still considered constant.

(ii) The initial concentrations of the unstable intermediate species that could not be measured were obtained from the information provided by Westerhoff et al.[56]

By way of example, the differential equation that describes the mass balance for the hydroxyl radical is the following:

$$R_{\bullet OH} = k_8\, C_{HO_3^\bullet} - k_9\, C_{O_3}\, C_{\bullet OH} - k_{10}\, C_{O_2^{-\bullet}}\, C_{\bullet OH} - k_{13}\, C_{HO_2^\bullet}\, C_{\bullet OH} - k_{14}\, C_{HO_3^\bullet}\, C_{\bullet OH} - k_{15}\, C_{H_2O_2}\, C_{\bullet OH} - k_{16}\, C_{HO_2^-}\, C_{\bullet OH} - k_{17}\, \left(C_{\bullet OH}\right)^2 - k_{20}\, C_{t-BuOH}\, C_{\bullet OH} \quad (16)$$

From the resolution of the system of 12 ODE, the following results were obtained:

Table 3. Concentration of •OH radicals in the presence of t-BuOH

Time	$C_{\bullet OH}$ (mol cm^{-3})
0 s	1×10^{-15} (a)
20 s	1.4×10^{-14} (b)
3 min.	1×10^{-20}
15 min.	1×10^{-25}
40 min.	1×10^{-30}
70 min.	1×10^{-35}
90 min.	1×10^{-40}
120 min.	1×10^{-45}
140 min.	1×10^{-50}

(a): Initializing concentration. (Taken from Westerhoff et al.[56]).
(b): Maximum value.

From Table 3, it can be observed that immediately after starting the reaction, the concentration of •OH radicals becomes very small (almost negligible). In this way, it can be considered that there are no •OH radicals in the solution and, as a reasonable approximation, it could not be necessary

to include the •OH radical species in the sequence of steps that will be used to study the direct ozonation by molecular ozone in the presence of t-BuOH.

With these results, the equations corresponding to the reaction of ozone with 2,4-D, 2,4-DCP and 2-CHQ were added to the original set. For this purpose, a reaction pathway which takes as its basis the mechanism published by Lovato et al.[36] can incorporate reactions (D), (E) and (F) as steps 21-23 in Table 2.

Steps (1) to (18) have reaction rate constants well known in the literature as indicated in Table 2. From these data, with the available experimental information, it is possible to solve the full system of differential equations together with a non-linear parameter estimator and, as a result of the optimization, obtain the values of k_{21} , k_{22} and k_{23}. From the optimization program, the following values for the three reactions were obtained:

$k_{21} = (1.00 \pm 0.09) \times 10^3$ cm^3 mol^{-1} s^{-1}

$k_{22} = (1.22 \pm 0.06) \times 10^4$ cm^3 mol^{-1} s^{-1}

$k_{23} = (3.37 \pm 0.02) \times 10^4$ cm^3 mol^{-1} s^{-1}

Figure 4 shows the correspondence between the experimental values and the results obtained from the simulation employing the proposed model and the obtained kinetic parameters. It can be observed that the agreement is quite good.

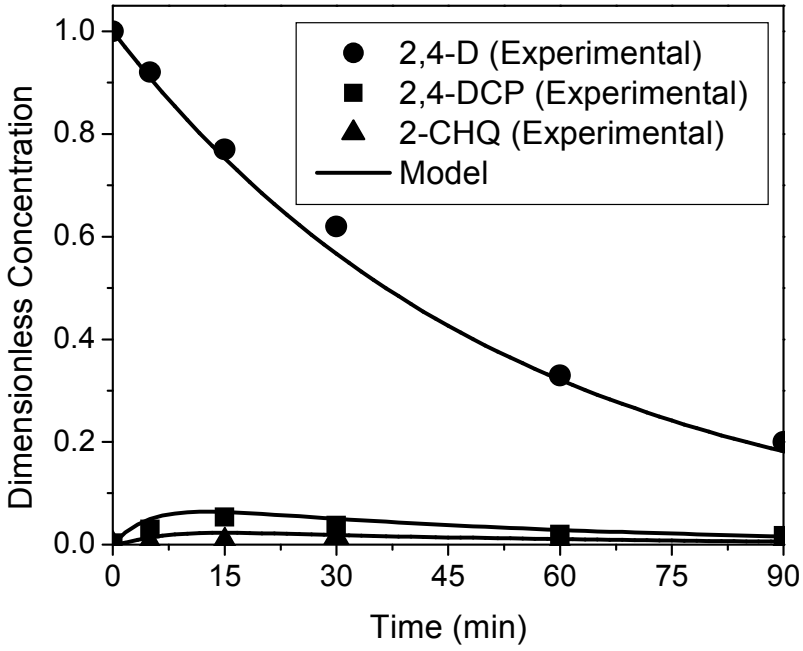

Figure 4. Direct reaction with molecular ozone. Comparison of simulation predictions with experimental data. $C_{O_3} = 3.18 \times 10^{-7}$ mol cm^{-3}

After 90 minutes of reaction, in the presence of t-BuOH, the direct ozonation is not able to complete the decomposition of 2,4-D. This could have been an expected result because molecular ozone possesses a high selectivity in its oxidative reactions and there is no doubt that the pollutant chemical structure requires the occurrence of much more active species for its entire degradation. Therefore, under acidic pH conditions, the effectiveness of molecular ozone acting separately and without the existence of highly reactive radicals, though not dispensable, cannot be considered very attractive.

5.2.2. Direct ozonation in the absence of t-BuOH

5.2.2.1. Experiments and data

After the steady state concentrations of ozone are reached $\left([O_3]_{s.s.}\right)$, the corresponding values are: 9.71×10^{-8}, 1.21×10^{-7} and 3.01×10^{-7} mol cm^{-3} (nominal values, accurately measured specifically for each case). 2,4-D initial concentrations were 1.79×10^{-6}, 1.70×10^{-6} and 1.78×10^{-6} mol cm^{-3}, respectively.

5.2.2.2. Reaction scheme and interpretation of the results

In this case, it is necessary to bear in mind that the ozone incorporated into the system is capable of oxidizing 2,4-D by the molecular track or through the radical formed from different series-parallel reactions. When using t-BuOH as scavenger, it was possible to eliminate the oxidation through the route with very active radicals and, therefore, the two effects could be separated. The reaction constants previously obtained (called k_{21}, k_{22} and k_{23}) are added to the mechanism described in Table 2 and in this case the reaction constants will be estimated exclusively for the interaction of the •OH radicals with 2,4-D, 2,4-DCP and 2-CHQ. Considering the reactions (I, J, K) as steps 24-26:

$$2,4-D + \bullet OH \rightarrow 2.4-DCP + Prod_7 \quad (I)$$

$$2,4-DCP + \bullet OH \rightarrow 2-CHQ + Prod_8 \quad (J)$$

$$2-CHQ + \bullet OH \rightarrow Prod_9 \quad (K)$$

Once more, the kinetic scheme corresponding to the 24 stages of reaction can be assembled (1-18 that describe the decomposition of ozone to include the generation of hydroxyl radicals, and 21-26 corresponding to the interaction of 2,4-D, 2,4-DCP and 2-CHQ with molecular ozone and •OH radicals, respectively) and solve the corresponding mass balances for the species involved. In combination with the non-linear multi- parameter estimator, the three kinetic constants can be calculated. The result yields:

$k_{24} = (4.00 \pm 0.23) \times 10^{11}$ cm^3 mol^{-1} s$^-$

$k_{25} = (7.58 \pm 0.59) \times 10^{12}$ cm^3 mol^{-1} s^{-1}

$k_{26} = (8.12 \pm 0.76) \times 10^{12}$ cm^3 mol^{-1} s^{-1}

The comparison of the estimated kinetic constants with the ones obtained for ozonation in the presence of t-BuOH shows that the presence of the hydroxyl radicals completely changes the progress of the reaction. This result is not surprising since the beneficial absence of selectivity in the oxidation capacity of the hydroxyl radicals and its high oxidizing potential could not produce a different outcome.

Figure 5 shows the agreement between experimental data and simulation results for one initial concentration of ozone. In view of these results at acidic pH, conditions are given for questioning the real importance of direct ozonation in the absence of the hydroxyl radicals. With the data obtained, the following reasoning is possible:

From Eq. (15), defining:

$$k_{overall} = k_{O_3}^{\oplus} + k_{\bullet OH}^{\oplus} \quad (17)$$

It can be obtained:

$$-\frac{d[2,4-D]}{dt} = k_{overall}[2,4-D] \quad (18)$$

The contribution of radical oxidation reactions to the overall 2,4-D degradation rate can be expressed as follows[53]:

$$\Delta_{\bullet OH} = \frac{k_{overall} - k_{O_3}^{\oplus}}{k_{overall}} \times 100 \quad (19)$$

Where $k_{overall}$ was defined above, and $k_{O_3}^{\oplus}$ was determined in the presence of t-BuOH, under the same operating conditions. For 2,4-D, 2,4-DCP and 2-CHQ, the kinetic contribution of radical reactions to complete degradation is 99.99%.

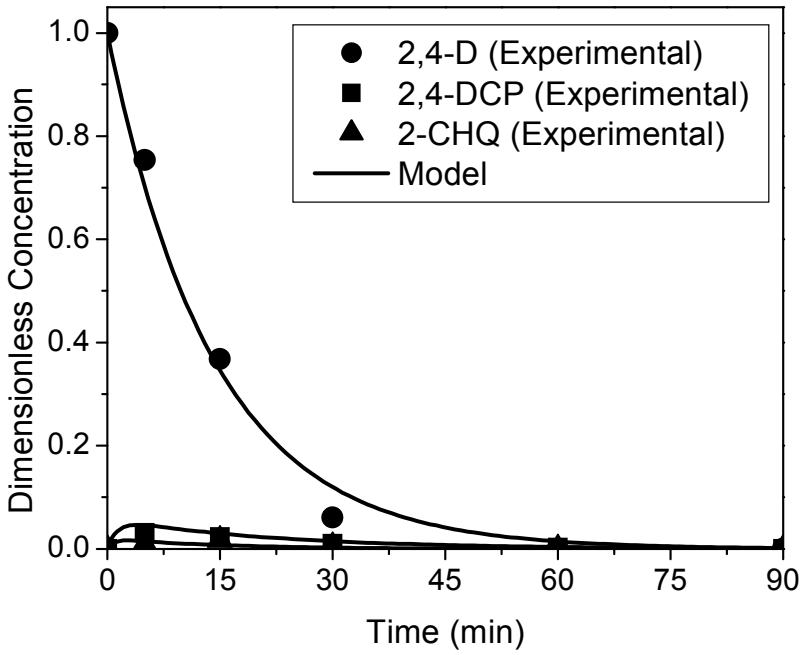

Figure 5. Reaction with ozone in the absence of t-BuOH. Comparison of simulation predictions with experimental data. $C_{O_3} = 3.01 \times 10^{-7}$ mol cm^{-3}.

5.3. Ozonation employing UVC radiation

5.3.1. Experiments and data

Two lamps were used in this part of the study (Philips TUV 15 W and Heraeus NNI 40 W). The incident radiation on the reactor walls were obtained by actinometric measurements, as described before. The concentrations of dissolved ozone were 9.3×10^{-8}, 1.21×10^{-7} and 1.93×10^{-7} mol cm^{-3} for the 15 W lamps, and 8.73×10^{-8}, 1.21×10^{-7} and 2.96×10^{-7} mol cm^{-3} for the 40 W lamps. The corresponding initial concentrations of 2,4-D were 1.54×10^{-6}, 1.70×10^{-6} and $1.70 \times$

10^{-6} mol cm^{-3} for the first case and 1.84×10^{-6}, 1.34×10^{-6} and 1.44×10^{-6} mol cm^{-3} for the second one.

The molar linear absorption coefficient of O_3 and H_2O_2 (formed from ozone photolysis, and immediately photolyzed into •OH radicals) are: 3.60×10^6 and 1.96×10^5 cm^2 mol^{-1}, respectively.

5.3.2. Reaction scheme and interpretation of the results

In this case one must be aware that ozone incorporated into the system is able to oxidize to 2,4-D by the molecular way (not very important, as previously shown) or through the •OH radicals formed from different reactions as described above. Moreover, the existing UVC radiation is also capable of reacting with 2,4-D, 2,4-DCP and 2-CHQ through photolysis, whose primary quantum yields were previously estimated. In addition, radiation is capable of acting on ozone producing hydrogen peroxide which will also decompose to give, as a result, an increase in the •OH radical concentration producing an effect of a similar nature to the rise of the pH.

The quantum yields of the photolytic reactions were obtained before. Those corresponding to the interaction of UVC with ozone and hydrogen peroxide are known from well-established references in the literature. Finally, the parameters corresponding to the different reactions of ozone and the •OH radicals with 2,4-D, 2,4-DCP and 2-CHQ were obtained in the previous sections.

Consequently, what remains to be done in this case is to gather all the processes involved so far, i.e., analyze whether the experimental performance is well represented by a simulation that includes all the corresponding steps, employing all constants already known or obtained in this work. To do so, one must proceed to compare predictions of the above mentioned simulations with new experimental values of the reaction carried out in the presence of ozone and UVC radiation acting simultaneously.

Consequently, the full sequence of reactions (1) to (18) in Table 2 must be taken and reactions (21) to (26) must be added as well as the photolysis reactions (A), (B) and (C), now called reactions (27) to (29), and reactions (30) to (31), corresponding to the photolysis of O_3 and H_2O_2

Table 4. Kinetic constants to complete the reaction scheme.

Step	Reaction	Kinetic Constant - units	Ref.
(21)	$2,4-D + O_3 \rightarrow 2.4-DCP + Prod_4$	$k_{21} = (1.00 \pm 0.09) \times 10^3$ cm^3 mol^{-1} s^{-1}	i
(22)	$2,4-DCP + O_3 \rightarrow 2-CHQ + Prod_5$	$k_{22} = (1.22 \pm 0.06) \times 10^4$ cm^3 mol^{-1} s^{-1}	ii
(23)	$2-CHQ + O_3 \rightarrow Prod_6$	$k_{23} = (3.37 \pm 0.02) \times 10^4$ cm^3 mol^{-1} s^{-1}	iii
(24)	$2,4-D + {}^{\bullet}OH \rightarrow 2.4-DCP + Prod_7$	$k_{24} = (4.00 \pm 0.23) \times 10^{11}$ cm^3 mol^{-1} s^{-1}	iv
(25)	$2,4-DCP + {}^{\bullet}OH \rightarrow 2-CHQ + Prod_8$	$k_{25} = (7.58 \pm 0.59) \times 10^{12}$ cm^3 mol^{-1} s^{-1}	v
(26)	$2-CHQ + {}^{\bullet}OH \rightarrow Prod_9$	$k_{26} = (8.12 \pm 0.76) \times 10^{12}$ cm^3 mol^{-1} s^{-1}	vi
(27)	$2,4-D \xrightarrow{h\nu} 2.4-DCP + Prod_1$	$\phi_{2,4-D}$=0.016 mol Einstein^{-1}	vii
(28)	$2,4-DCP \xrightarrow{h\nu} 2-CHQ + Prod_2$	$\phi_{2,4-DCP}$ = 0.017 mol Einstein^{-1}	viii
(29)	$2-CHQ \xrightarrow{h\nu} Prod_3$	ϕ_{2-CHQ} = 0.041 mol Einstein^{-1}	ix
(30)	$O_3 + H_2O \xrightarrow{h\nu} H_2O_2 + O_2$	ϕ_{O_3} = 0.50 mol Einstein^{-1}	64
(31)	$H_2O_2 \xrightarrow{h\nu} 2\ {}^{\bullet}OH$	$\phi_{H_2O_2}$ = 0.48 mol Einstein^{-1}	65

i, ii, iii, iv, v, vi, vii, viii and ix: this work.

As in previous cases, the differential equations describing the time evolution of all reagents, reaction intermediates and reaction products must be developed. The previously known kinetic constants as well as the new ones determined in this work are used in the whole set of ODE. When applicable, the equations that describe the volumetric rate of absorption of photons of each one of the species capable of absorbing UV radiation must be added.

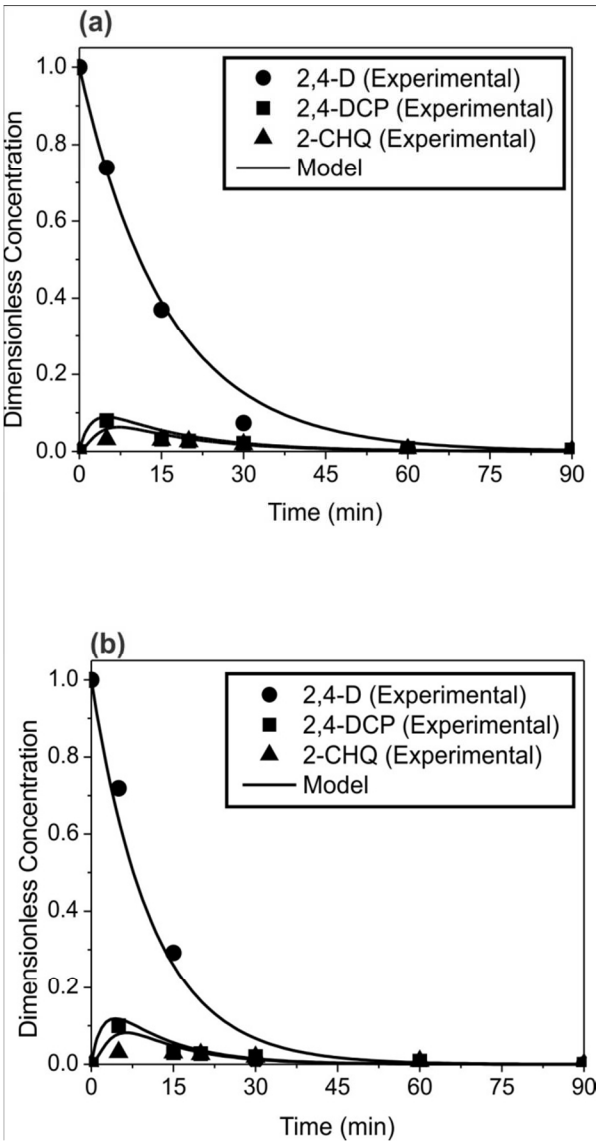

Figure 6. Results of the complete kinetic sequence. $C_{O_3} = 1.21 \times 10^{-7}$ mol cm^{-3}. (a) Lamp: Nominal input power = 15W. (b) Lamp: Nominal input power = 40W.

With these data, without making any further adjustment of parameters, the results that are shown in Figure 6 (a) and (b) are obtained for two different irradiation conditions.

Two conclusions can be immediately drawn: (i) The system of 29 steps (see Table 2 and Table 4) seems to describe the performance of the reaction system; also, all the compounds enclosed in the generic denomination of "Products" do not interfere with the disappearance rate of the principal

reaction species, i.e. 2,4-D, 2,4-DCP and 2-CHQ, and (ii) the effect of increasing the magnitude of the existing radiation field is significant. In fact, the decomposition of the three species requires 90 minutes with the 15 W power input lamp and only 60 minutes with the more powerful lamp (40W). Yet, another significant result is that the proposal of the kinetic separation of specific rate constants (21) to (23) from the ones corresponding to steps (24) to (26) sounds correct, because the second set did not need any adjustment when the UVC radiation was added to the system. Simulation results indicate that the change in •OH concentration varies from one to two orders of magnitude when the lamps are added to the system. Part of the merit of the quality of these values (that also include the ones corresponding to the photolytic reactions) resides in the evaluation of the radiation field according to Eq. (2) and also to the proper definition of the averaging integral.

5.3.3. Detailed description of the existing radiation field

With regard to the radiation field, the first thing that must be noted is that the rate of absorption of photons, as shown in Eq. (2) is not only proportional to the absorption coefficient of the particular reacting species taken into consideration, but also involves in its definition the rest of the chemical species that are in the system and can participate in the process of radiation absorption. That is specifically indicated in the exponential part of Eq. (2). Secondly, the volume averaged LVRPA is not the result of an actinometric global measurement of the total number of photons that exists in the reactor divided by its volume. It is the integration of the "local values" of the LVRPA over the volume of the reactor divided by the above mentioned volume, which is not the same, as explained by Eq. (2).

These aspects are better visualized in Figure 7 where the field generated by each significant species present in the reactor volume is shown, as well as the total field produced by the presence of all species, the last one for two different ozone concentrations.

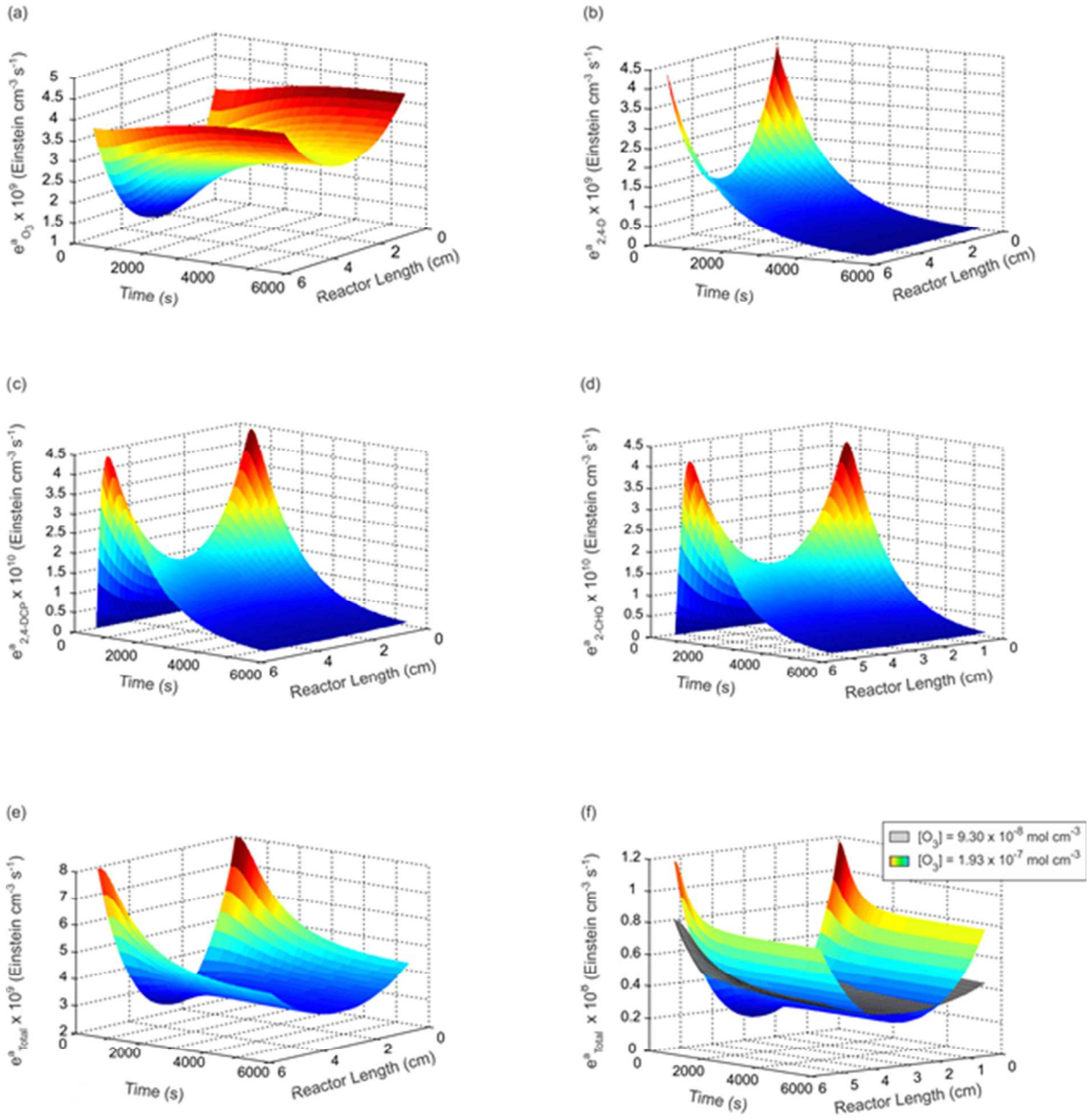

Figure 7. LVRPA as a function of time and reactor length: (a) ozone, (b) 2,4-D, (c) 2,4-DCP and (d) 2-CHQ; (e) Total local volumetric rate of photon absorption. $C_{O_3} = 1.93\times 10^{-7}$ mol cm^{-3} for all these figures; (f) Effect of different ozone concentration, $C_{O_3} = 9.30\times 10^{-8}$ mol cm^{-3} and 1.93×10^{-7} mol cm^{-3}. Lamp: 40W in all cases.

In all cases, the reaction time and the reactor radius are used as independent variables in a three dimensional representation. It should be noted that all figures with the exception of the one corresponding to pure ozone are a function of time because concentrations are a function of time.

Figure 7 (a) clearly shows that in spite of the fact that ozone concentration remains constant all the time, its value of the LVRPA changes by the presence of other components that absorb radiation and only becomes constant when all of them have practically disappeared. And in the same way, Figure 7 (b) shows that when all 2,4-D has disappeared, its LVRPA becomes zero. Figure 7 (c) and (d) shows how a rigorous modeling of the radiation field allows observing the effects that produce the occurrences of the major reaction by-products. Each one of them defines their own photon absorption rate according to their concentrations, their own molar absorption coefficients and the existence of other compounds that influence the complete environment. Figure 7 (e) and (f) reveals that in practice the shape of the entire field of radiation energy is controlled by ozone, be it for its high absorption coefficient or, much specifically, for its concentration that remains constant.

5.3.4 Ozonation at neutral and alkaline pH

Three additional sets of runs were carried out working with the highest concentration of ozone (always in the order of 2.9×10^{-7} mol cm^{-3}) and using the two 40 W lamps: (i) at pH 10 without a buffer solution, (ii) at pH 7 with a buffer solution and (iii) at pH 10 with a buffer solution.

Working without buffering, the pH of the reaction very rapidly falls to values close to 3, whereupon the obtained experimental curve is almost the same as that working at the natural, original pH of the solution. The model developed before explains why, working without buffering, all the results are the same. It seems that when beginning at pH 7, the concentration of the OH^- anion reaches a value of 10^{-14} mol cm^{-3} (10^{-11} M) falling down to pH = 3 in 3.2 minutes. Similarly, in the case of starting at pH 10, after 4.65 minutes the pH also decreases to a value equal to 3. It also shows that the degradation of the 2,4 -D is almost not affected by this way of modifying the pH. Consequently, it can be concluded that when the ozonation has been enhanced

by the presence of UVC radiation, in the absence of a buffer solution, the change in the pH has almost no effect, mainly because the pH evolves fast and spontaneously towards the initial pH of the solution.

In the results shown along the previous sections, starting from the pH corresponding to the solution of 2,4-D in water (a value around 3) the proposed model predicts that the concentrations of H^+ and OH^- change according to the progress of the reaction.

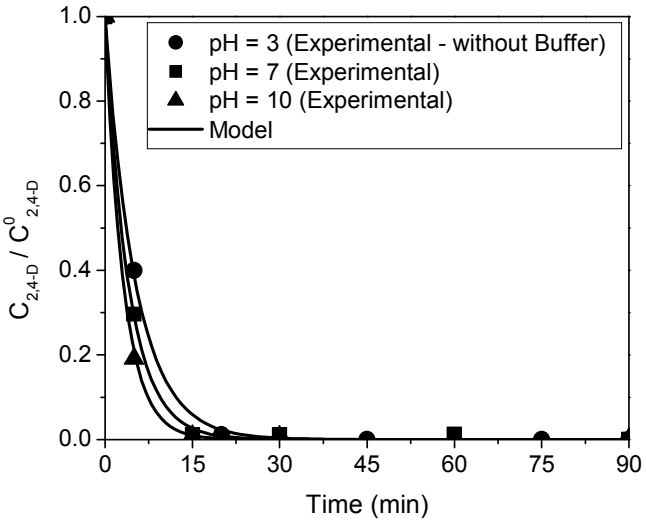

Figure 8. Effect of modification of the pH. Ozone concentration=2.9 $\times 10^{-7}$ mol cm^{-3}. Lamps: Nominal input power=40W in all cases. Data at pH 7 and 10, employing buffer solutions

On the other hand, when a buffer solution is used, the concentrations of H^+ and OH^- are forced to remain constant. In that case, the evolution of 2,4 -D will be affected in the way shown in Figure 8. When the pH is kept constant, either at pH of 7 or 10, the degradation rate of 2,4-D increases during the first 15 minutes. Beyond this time, in all three cases, almost all 2,4-D has been consumed. Looking at the results, after 5 minutes of reaction time, starting with pH = 7 and working with the buffer solution, the conversion of 2.4-D is increased by 26%. Even more

ostensible, at the same time, starting with a pH = 10 and also employing the buffer solution, the degradation rate is enlarged by 52%.

The model can also be used to calculate the concentration of the •OH radicals at every pH. At pH = 3, the maximum calculated concentration of •OH radicals is 1×10^{-15} mol cm^{-3}, at pH 7 is 1×10^{-12} mol cm^{-3} and in the case of pH = 10, it is 1×10^{-11} mol cm^{-3}. These values explain why the model also represents the values of 2,4-D degradation at three different pHs without any modification of the kinetic constants. Changes in the concentration of the •OH radicals that are described by the model explain the variation in the decomposition rates.

6. GLOBAL KINETIC RESULTS

6.1. Final values of TOC

Even in the case under which the operating conditions used in the reactor correspond to the highest values of ozone concentration and of incident radiation studied ($C^0_{2,4-D} = 1.44 \times 10^{-6}$ mol cm^{-3}, $C^0_{O_3} = 2.96 \times 10^{-7}$ mol cm^{-3}, $G_W = 4.81 \times 10^{-8}$ Einstein $cm^{-2}s^{-1}$), it can be noted that the reaction turns out to be slow to obtain an entire mineralization. In Figure 9, it can be observed that 10 hours are needed to reach it. It should be noted that after 4 hours of reaction, the reduction of TOC is about 91%. Then, 6 additional hours are required to complete mineralization. In any event, with or without full mineralization, the final word as far as water quality is concerned, will be given by standard toxicity essays.

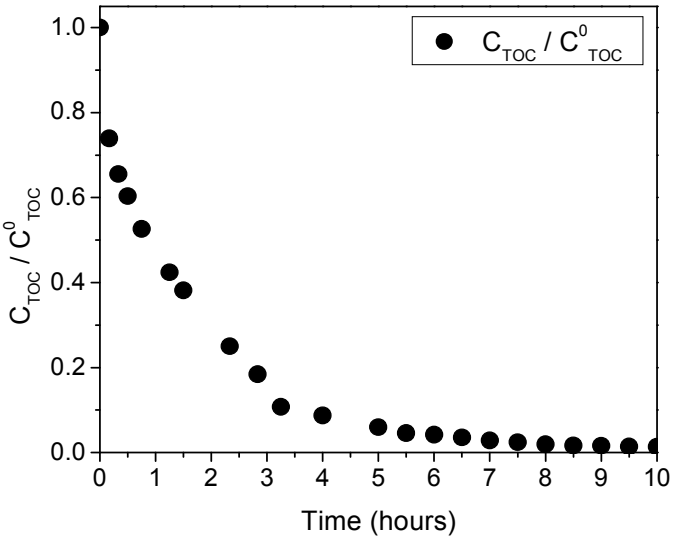

Figure 9. TOC reduction.

6.1.1. A comment concerning very long mineralization times

From the displayed results it is clear that the reaction exhibits a faster stage (without it being exceedingly fast) and another which is extremely slow. As shown in Figure 9, up to about three to four hours - depending on the operating conditions- a mineralization of the order of 90% is obtained. Then, six additional hours are necessary to achieve complete oxidation. As expressed below, there is an explanation for this phenomenon. But it is clear that it is unavoidable to think whether or not there is the possibility of combining - without changing the process - two different operating conditions employing two reactors in series for each of them. Or, perhaps, alternatively, analyze if it is feasible to carry out the proposed task with two different processes for each of the two stages that are so dissimilar. A third alternative - not unquestionably the best - would be to put an end to the action at the moment when toxicity essays conducted in parallel indicate that water has lost all its dangerousness although the proposed entire mineralization has not been achieved.

Concerning the results plotted in Figure 9, it seems appropriate to remark that measures of TOC are useful to evaluate to what extent the oxidation process has succeeded in the completeness of its objective, but it is not a suitable variable for monitoring reaction rates. Some compounds may have disappeared completely from the reacting system and the value of the TOC measured at that time remains invariant because the carbon that turned to be a part of another species continues in its organic form.

Nevertheless, what in Figure 9 looks like a two-stage kinetics having different reaction rates is the result of a process that after the disappearance of all chlorinated derivatives and the existing double C=C bonds gives rise to the production of carboxylic acids (single bounded) that are much more difficult to oxidize. At the beginning, the reactions that breakdown 2,4-D, 2,4-DCP, 2-CHQ as well as other chlorinated intermediaries are relatively fast. When this stage ends, which is quite clear because the production of chloride ions reaches an ostensible steady state, as will be shown later, there are still many non-chlorinated compounds and some open chain acids that are significantly slower in their degradation and consequently, will maintain the existence of high values of TOC.

Although the effect of the addition of radiation and the rise of the pH (but holding it constant with the inclusion of a buffer solution) change the reaction rate notoriously, their favorable effects are not linear. The passage of the lamp power from 15 to 40 W does not cause a significantly equivalent improvement in the final output. The modification of the pH (from 3 to 7 and to 10) shows a highly positive effect on the first part of the reaction (no longer than half an hour) and then, the entire process follows virtually the same course as when lower pHs were used. Changes in these two variables that are intended to increase the concentration of hydroxyl radicals soon find a limit in their effects. Nothing too different should be expected by attempting to apply an appreciably larger concentration of ozone. The effect will be almost the same. For

this reason, a large increase in the concentration of ozone or a change of the used lamps to nominal input powers above 40 W, does not seem to be the operational variable whose modification can make a substantial contribution to solve the problem of the long times required to obtain total mineralization of 2,4-D. This is also very important when one bears in the mind the cost that involves each of the mentioned alternatives.

Instead, could be a possible economic solution that has been widely used as a complement to many the AOPs is to transfer the operation to a biological process operated in series from the moment when the rate falls down and the BOD has acquired the value that could ensure a viable solution[66].

6.2. Production of chloride ion: dechlorination

Mineralization of 2,4-D leads to the loss of chlorine atoms of its aromatic ring. A complete kinetic mechanism would predict that, after complete degradation, 2 mols of HCl must be formed for each mol of 2,4-D that decomposes. The overall rate of dechlorination was followed by measuring the concentration of Cl^- (chloride ion) accumulated in the solution, and is presented in Figure 10 (a) and (b).

As it can be observed, at the end of the reaction, when all 2,4-D and its chloroaromatic derivatives have been removed (after only 90 min), the molar relationship $C_{Cl^-}/C^0_{2,4-D}$ is 1.99, which is an indication that the ozonation process produces the dechlorination of all the involved pollutants, with a full increase in the expected theoretical equivalent of chloride ion formation.

This is a stable species that acidifies the reacting medium in agreement with our experimental observations. This result is very important because when all chlorinated compounds have been decomposed, very likely a significant part of the pollutant toxicity has been removed.

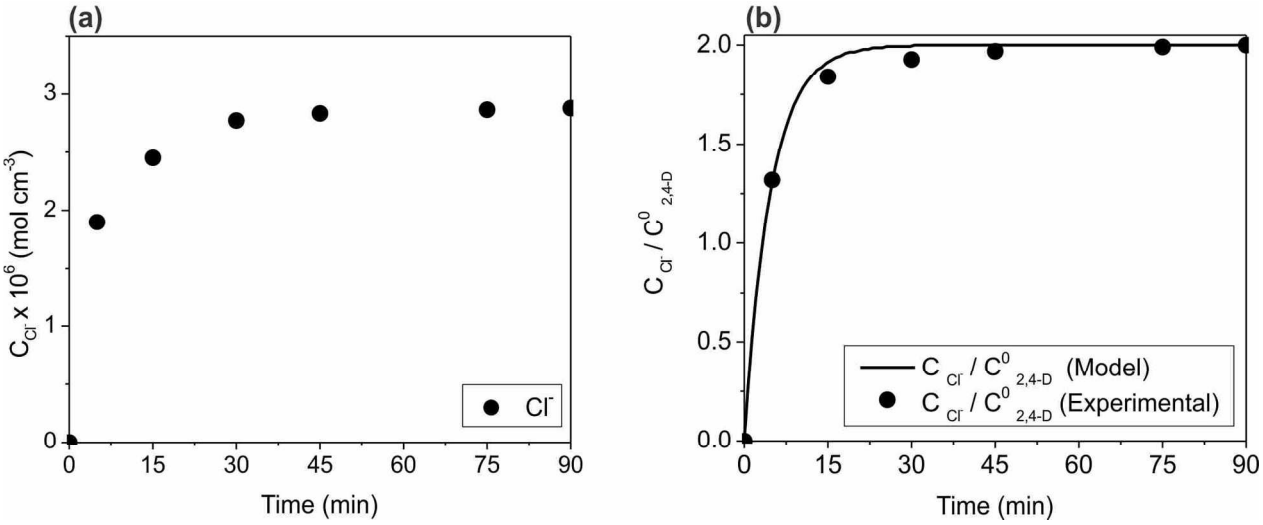

Figure 10. (a) Chloride ion concentration and (b) Ratio of chloride ion formation with respect to 2,4-D decomposition: experimental and theoretical results.

7. CONCLUSIONS

A fairly complete and rigorous kinetic model for the decomposition of 2,4-D and its two main decomposition products, namely 2,4-DCP and 2-CHQ, using ozone with and without the presence of UVC radiation has been developed. The model includes (i) direct photolysis, (ii) isolated molecular ozone attack, (iii) reaction when ozone acts in the presence of the hydroxyl radicals that produces its own decomposition, (iv) enhanced reaction rate when UVC radiation is incorporated inside the reactor and (v) changes in 2,4-D conversion when the pH is raised to 7 and 10.

The description of the system resorts to a reaction scheme with 29 steps and their corresponding 29 kinetic constants, nine of which were determined in this work in a progressive way (never more than three at a time). The mathematical model developed very well represents the experimental data when the work is carried out in the natural pH resulting from the concentrations of the contaminant used in this work.

The results of the direct photolysis indicate that these reactions are not of great importance. Isolating the action of molecular ozone oxidation, eliminating the presence of the hydroxyl radicals that might be present (through their trapping with t-BuOH) it could be observed that this reaction, although giving clearly detectable conversions, does not reach sufficiently prominent and useful results, when they are compared with the case in which ozone acts in the company of hydroxyl radicals which are produced during its own decomposition. The change in the throughput under these conditions is truly significant. Finally, the presence of not very high levels of UVC radiation increases the process rate remarkably.

Resorting to the inclusion of buffer solutions, the pH of the reaction was increased up to values of 7 and 10. The rate of decomposition of 2,4-D was significantly increased to values substantially beyond those achieved with the enhancement resulting from incorporating UVC radiation. Nevertheless, this raise in the pH does not decrease the time required to achieve complete mineralization, because after the brief initial period that shows the improvement mentioned above, the reaction continues its subsequent steps in the same way as at pH = 3.

Working in the most appropriate range of operating conditions within the span of the explored variables, this approach only achieved complete mineralization after almost ten hours of reaction. Nevertheless, before the process completed ninety minutes of reaction, all the chlorinated compounds had been decomposed and the balance of chlorine theoretically separated from the organic compounds liberating chlorides into the solution, closed within an error smaller than 3 %.

The model includes a very accurate description of the reaction and the radiation field existing at each time and their exact quantification is part of the mathematical description that represents the developed kinetics.

In brief, a comprehensive kinetic model has been developed which is so robust that when the operating conditions are substantially modified, either because they may comprise UVC radiation

or not, or the pH is subjected to extensive alterations, it does not need to change any of its 29 reaction steps which describe the reaction or the corresponding values of specific rate constants. This emanates from a precise discrimination and quantification of the involved reactions. In other words, rightfully combining mass and radiation balances whatever the source of formation of the hydroxyl radicals is, the model is able to represent the progress of the reaction without demanding changes in the involved concepts or the addition of empirically adjustable parameters. These results, which from the method devised in their production have an intrinsic character, are completely suitable to perform a scaling-up or reactor design at the desired size and configuration.

Acknowledgments

The authors are grateful to Universidad Nacional del Litoral (UNL), Consejo Nacional de Investigaciones Científicas y Técnicas (CONICET), and Agencia Nacional de Promoción Científica y Tecnológica (ANPCyT) for the financial support.

Supporting Information Available: The corresponding emission spectra and additional data of the lamps and reacting system, complementary information regarding the experimental procedures and analytical methods, GC-MS spectra of identified intermediate derivatives, and additional details about the reactor mass balance and the radiation model can be found in the Supporting Information. This information is available free of charge via the Internet at http://pubs.acs.org/.

Notation

2,4-D	2,4-Dichlorophenoxyacetic acid
2,4-DCP	2,4- Dichlorophenol
2-CHQ	2- Chlorohydroquinone
t-BuOH	Tert-butanol
C	Concentration (mol cm^{-3})
X	Cartesian spatial coordinate (cm)
L	Length (cm)
V	Volume (cm^3)
G	Incident Radiation (Einstein cm^{-2} s^{-1})
e^a	Local volumetric rate of photon absorption (Einstein cm^{-3} s^{-1})
K	Kinetic constant. (Units vary with the reaction order)
R	Reaction rate (mol cm^{-3} s^{-1})
k_L a	Volumetric mass transfer coefficient (s^{-1})
T	Time (s)

Greek Letters

κ	Linear Napierian absorption coefficient (cm^{-1})
λ	Wavelength (nm)
ϕ	Primary quantum yield (mol $Einstein^{-1}$)

Subscripts

λ	Relative to radiation of wavelength λ

I	Relative to the "i" reactive energy-absorbing species
J	Relative to all radiation-absorbing species (including catalysts or inner filtering species)
R	Relative to the photoreactor
W	Relative to the reactor window
Tot	Denotes total volume
Irr.	Relative to irradiated volume
D	Relative to dark volume
O_3	Relative to Ozone
•OH	Relative to •OH radical
2,4-D	Relative to 2,4-Dichlorophenoxyacetic acid
2,4-DCP	Relative to 2,4- Dichlorophenol
2-CHQ	Relative to 2- Chlorohydroquinone
t-BuOH	Relative to Tert-butanol
Ss	Relative to Stationary State

Superscripts

0	Relative to the initial time (t = 0)

Special Symbols

$\langle \circ \rangle$	Represents a volume average over a defined space

References

(1) Vanden Bilcke, C. The Stockholm Convention on Persistent Organic Pollutants. *R.E.C.I.E.L.* **2002**, *11*, 328.

(2) Kidd, H.; James, D. R. The Agrochemicals Handbook, Third Edition. Royal Society of Chemistry Information Services, Cambridge, 1991

(3) Colina-Márquez, J.; Machuca-Martínez, F.; Li Puma, G. Photocatalytic Mineralization of Commercial Herbicides in a Pilot-Scale Solar CPC Reactor: Photoreactor Modeling and Reaction Kinetics Constants Independent of Radiation Field. *Environ. Sci. Technol.* **2009***, 43,* 8953.

(4) Guzmán, C.; del Ángel, G.; Gómez, R.; Galindo-Hernández, F.; Ángeles-Chavez, C. Degradation of the Herbicide 2,4-Dichlorophenoxyacetic Acid Over $Au/TiO_2–CeO_2$ Photocatalysts: Effect of the CeO_2 Content on the Photoactivity. *Catal. Today* **2011**, *166*, 146.

(5) Fontmorin, J.M.; Huguet, S.; Fourcade, F.; Geneste, F.; Floner, D.; Amrane, A. Electrochemical Oxidation of 2,4-Dichlorophenoxyacetic Acid: Analysis of By-Products and Improvement of the Biodegradability. *Chem. Eng. J.* **2012**, *195–196*, 208.

(6) Chen, L.; Li, Z.; Quan, Y.; Fang, D. Ozone Treatment of Soil Contaminated with Chlorinated Herbicides. *2nd International Conference on Remote Sensing, Environment and Transportation Engineering Proceedings.* **2012**, art. N° 6260651.

(7) Peller, J.; Wiest, O.; Kamat, P. V. Hydroxyl Radical's Role in the Remediation of a Common Herbicide, 2,4-Dichlorophenoxyacetic Acid (2,4-D). *J. Phys. Chem. A*. **2004**, *108*, 10925.

(8) Celis, E.; Elefsiniotis, P.; Singhal, N. Biodegradation of Agricultural Herbicides in Sequencing Batch Reactors under Aerobic or Anaerobic Conditions. *Water Res.* **2008**, *42*, 3218.

(9) Vroumsia, T.; Steiman, R.; Seigle-Murandi, F.; Benoit-Guyod, J. L. Fungal Bioconversion of 2,4-Dichlorophenoxyacetic Acid (2,4-D) and 2,4-Dichlorophenol (2,4-DCP). *Chemosphere* **2005**, *60*, 1471.

(10) Chu, W.; Kwan, C. Y.; Chan, K. H.; Chong, C. An Unconventional Approach to Studying the Reaction Kinetics of the Fenton's Oxidation of 2,4-Dichlorophenoxyacetic Acid. *Chemosphere* **2004**, *7*, 1165.

(11) Mendoza-Marín, C.; Osorio, P.; Benítez, N. Decontamination of Industrial Wastewater from Sugarcane Crops by Combining Solar Photo-Fenton and Biological Treatments. *J. Hazard. Mater.* **2010**, *177*, 851.

(12) Badellino, C.; Arruda Rodrigues, C.; Bertazzoli, R. Oxidation of Pesticides by in Situ Electrogenerated Hydrogen Peroxide: Study for the Degradation of 2,4-Dichlorophenoxyacetic Acid. *J. Hazard. Mater.* **2006**, *137*, 856.

(13) Galindo-Hernández, F.; Gómez, R. Degradation of the Herbicide 2,4-Dichlorophenoxyacetic Acid over TiO_2–CeO_2 Sol–gel Photocatalysts: Effect of the Annealing Temperature on the Photoactivity. *J. Photoch. Photobio. A.* **2011**, *217*, 383.

(14) Mohamed, M. M.; Khairou, K. S. Preparation and Characterization of Nano-Silver/ Mesoporous Titania Photocatalysts for Herbicide Degradation. *Micropor. Mesopor. Mat*. **2011**, *142*, 130.

(15) Seck, E. I.; Doña-Rodríguez, J. M.; Fernández-Rodríguez, C.; González-Díaz, O. M.; Araña, J.; Pérez-Peña, J. Photocatalytic Removal of 2,4-Dichlorophenoxyacetic Acid by Using Sol–gel Synthesized Nanocrystalline and Commercial TiO_2: Operational Parameters Optimization and Toxicity Studies. *Appl. Catal. B-Environ*. **2012**, *125*, 28.

(16) Rivera-Utrilla, J.; Sánchez-Polo, M.; Abdel daiem, M. M.; Ocampo-Pérez, R. Role of Activated Carbon in the Photocatalytic Degradation of 2,4-Dichlorophenoxyacetic Acid by the UV/TiO_2/ Activated Carbon System. *Appl. Catal. B-Environ*. **2012**, *126*, 100.

(17) Alfano, O. M.; Brandi, R. J.; Cassano, A. E. Degradation Kinetics of 2,4-D in Water Employing Hydrogen Peroxide and UV Radiation. *Chem. Eng. J.* **2011**, *82*, 209.

(18) Chu, W.; Chan, K. H.; Kwan, C. Y. Modeling the Ozonation of Herbicide 2,4-D through a Kinetic Approach. *Chemosphere* **2004**, *55*, 647.

(19) Tsyganok, A. I.; Yamanaka, I.; Otsuka, K. Dechlorination of Chloroaromatics by Electrocatalytic Reduction over Palladium-Loaded Carbon Felt at Room Temperature. *Chemosphere* **1999**, *39*, 1819.

(20) Peller, J.; Wiest, O.; Kamat, P. Synergy of Combining Sonolysis and Photocatalysis in the Degradation and Mineralization of Chlorinated Aromatic Compounds. *Environ. Sci. Technol.* **2003**, *37*, 1926.

(21) Zona, R.; Solar, S.; Gehringer, P. Degradation of 2,4-Dichlorophenoxyacetic Acid by Ionizing Radiation: Influence of Oxygen Concentration. *Water Res.* **2002**, *36*, 1369.

(22) Homlok, R.; Takacs, E.; Wojnarovits, L. Radiolytic Degradation of 2,4-Dichlorophenoxyacetic Acid in Dilute Aqueous Solution: pH Dependence. *J. Radioanal. Nucl. Chem*. **2010**, *284*, 415.

(23) Solpan, D.; Torun, M. The Removal of Chlorinated Organic Herbicide in Water by Gamma - Irradiation. *J. Radioanal. Nucl. Chem*. **2012**, *293*, 21.

(24) Piera, E; Calpe, J. C.; Brillas, E.; Domènech, J.; Peral, J. 2,4-Dichlorophenoxyacetic Acid Degradation by Catalyzed Ozonation:TiO_2/UVA/O_3 and Fe(II)/UVA/O_3 Systems. *Appl. Catal. B-Environ*. **2000**, *27*, 169.

(25) Chu, W.; Ching, M. H. Modeling the Ozonation of 2,4-Dichlorophoxyacetic Acid through a Kinetic Approach. *Water Res.* **2003**, *37*, 39.

(26) Benitez, F. J.; Acero, J. L; Real, F. J.; Roman, S. Oxidation of MCPA and 2,4-D by UV Radiation, Ozone, and the Combinations UV/H_2O_2 and O_3/H_2O_2. *J. Environ. Sci. Heal. B.* **2004**, *3*, 393.

(27) Alvarez, M; López, T; Odriozola, J. A.; Centeno, M. A.; Domínguez, M. I.; Montes, M.; Quintana, P.; Aguilar, D. H.; González, R. D. 2,4-Dichlorophenoxyacetic Acid (2,4-D) Photodegradation Using an Mn+/ZrO_2 Photocatalyst: XPS, UV−Vis, XRD Characterization. *Appl. Catal. B-Environ.* **2007**, *73*, 34.

(28) Yu, Y.; Ma, J.; Hou, Y. Degradation of 2,4-Dichlorophenoxyacetic Acid in Water by Ozone-Hydrogen Peroxide Process. *J. Environ. Sci.* **2006**, *18*, 1043.

(29) Giri, R. R.; Ozaki, H.; Ishida, T.; Takanami, R.; Taniguchi, S. Synergy of Ozonation and Photocatalysis to Mineralize Low Concentration 2,4-Dichlorophenoxyacetic Acid in Aqueous Solution. *Chemosphere* **2007***, 66,* 1610.

(30) Giri, R. R.; Ozaki, H.; Ishida, T.; Taniguchi, S.; Takanami, R. Photocatalytic Ozonation of 2,4-Dichlorophenoxyacetic Acid in Water with a New TiO_2 Fiber. *Int. J. Environ. Sci. Tech*. **2008**, *5*, 17.

(31) Oyama, T.; Yanagisawa, I.; Takeuchi, M.; Koike, T.; Serpone, N.; Hidaka, H. Remediation of Simulated Aquatic Sites Contaminated with Recalcitrant Substrates by TiO_2 /Ozonation under Natural Sunlight. *Appl. Catal. B-Environ*. **2009**, *91*, 242.

(32) Xing, S.; Hu, C.; Qu, J.; He, H.; Yang, M. Characterization and Reactivity of MnO*x* Supported on Mesoporous Zirconia for Herbicide 2,4-D Mineralization with Ozone. *Environ. Sci. Technol.* **2008**, *42,* 3363.

(33) Hu, C.; Xing, S.; Qu, J.; He, H. Catalytic Ozonation of Herbicide 2,4-D over Cobalt Oxide Supported on Mesoporous Zirconia. *J. Phys. Chem. C* **2008,** *112,* 5978.

(34) Lopez-Lopez, A.; Pic, J. S.; Debellefontaine, H. Ozonation of Azo Dye in a Semi-Batch Reactor: A Determination of the Molecular and Radical Contributions. *Chemosphere* **2007**, *66*, 2120.

(35) Lovato, M. E.; Martín, C. A.; Cassano, A. E. Degradation of Dichloroacetic Acid in Homogeneous Aqueous Media Employing Ozone and UVC Radiation. *Photochem. Photobiol. Sci.* **2011**, *10*, 367.

(36) Lovato, M. E.; Martín, C. A.; Cassano, A. E. A Reaction–Reactor Model for O_3 and UVC Radiation Degradation of Dichloroacetic Acid: The Kinetics of Three Parallel Reactions. *Chem. Eng. J.* **2011**, *171*, 474.

(37) Cassano, A. E.; Martín, C. A.; Brandi, R. J.; Alfano, O. M. Photoreactor Analysis and Design: Fundamentals and Applications. *Ind. Eng. Chem. Res.* **1995**, *34*, 2155.

(38) Brillas, E.; Calpe, J. C.; Casado, J. Mineralization of 2,4-D by Advanced Electrochemical Oxidation Processes. *Water Res.* **2000**, *34,* 2253.

(39) Hoigné, J.; Bader, H. Rate Constants of Reactions of Ozone with Organic and Inorganic Compounds in Water—I: Non-Dissociating Organic Compounds. *Water Res.* **1983**, *17*, 173.

(40) Llompart, M.; Lourido, M.; Landín, P.; García-Jares, C.; Cela, R. Optimization of a Derivatization-Solid-Phase Microextraction Method for the Analysis of Thirty Phenolic Pollutants in Water Samples. *J. Chromatogr. A* **2002**, *963*, 137.

(41) Bader, H.; Hoigné, J. Determination of Ozone in Water by the Indigo Method. A Submitted Standard Method. *Ozone: Sci. Eng.***1982**, *4*, 169.

(42) Murov, S.; Carmichael, I.; Hayon, G. *Handbook of Photochemistry*; Marcel Dekker: New York, 1993.

(43) Zalazar, C. S.; Labas, M. D.; Martín, C. A.; Brandi, R. J.; Alfano, O. M.; Cassano, A. E. The Extended Use of Actinometry in the Interpretation of Photochemical Reaction Engineering Data. *Chem. Eng. J.* **2005**, *109*, 67.

(44) Brillas, E.; Calpe, J. C.; Cabot, P. Degradation of the Herbicide 2,4-Dichlorophenoxyacetic Acid by Ozonation Catalyzed with Fe^{2+} and UVA Light. *Appl. Catal. B* **2003**, *46,* 381.

(45) Brillas, E.; Cabot, P. L.; Rodríguez, R. M.; Arias, C.; Garrido, J. A.; Oliver, R. Degradation of the Herbicide 2,4-D by Catalyzed Ozonation Using the O_3/Fe^{2+}/UVA System. *Appl. Catal. B-Environ.* **2004**, *51*, 117.

(46) Peller, J.; Wiest, O.; Kamat, P. Sonolysis of 2,4-Dichlorophenoxyacetic Acid in Aqueous Solutions. Evidence for OH Radical Mediated Degradation. *J. Phys. Chem. A* **2001,** *105,* 3176.

(47) Peller, J.; Wiest, O.; Kamat, P. Radiolytic Transformations of Chlorinated Phenols and Chlorinated Phenoxyacetic Acids. *J. Phys. Chem. A* **2005**, *109,* 9528.

(48) Gao, J.; Zhao, G.; Shi, W.; Li, D. Microwave Activated Electrochemical Degradation of 2,4-Dichlorophenoxyacetic Acid at Boron-Doped Diamond Electrode. *Chemosphere* **2009**, *75*, 519.

(49) Xiao, H.; Liu, R.; Zhao, X.; Qu, J. Effect of Manganese Ion on the Mineralization of 2,4-Dichlorophenol by Ozone. *Chemosphere* **2008**, *72*, 1006.

(50) Boudart, M.; Djéga-Mariadassou, G. *Kinetics of Heterogeneous Catalytic Reactions;* Princeton University Press: Princeton, 1984.

(51) von Gunten, U. Ozonation of Drinking Water: Part I, Oxidation Kinetics and Product Formation. *Water Res*. **2003**, *37*, 1443.

(52) Astarita, G.; Savage, D.; Bisio, A. *Gas Treating with Chemical Solvents;* John Wiley and Sons Inc.: New York, 1983.

(53) Ferreira de Oliveira, T.; Chedeville, O.; Fauduet, H.; Cagnon, B. Use of Ozone/Activated Carbon Coupling to Remove Diethyl Phthalate from Water: Influence of Activated Carbon Textural and Chemical Properties. *Desalination* **2011***, 276,* 359.

(54) Fábián, I. Reactive Intermediates in Aqueous Ozone Decomposition: A Mechanistic Approach. *Pure Appl. Chem*. **2006**, *78*, 1559.

(55) Tomiyasu, H.; Fukutomi, H.; Gordon, G. Kinetics and Mechanism of Ozone Decomposition in Basic Aqueous Solution. *Inorg. Chem.* **1985***, 24*, 2962.

(56) Westerhoff, P.; Song, R.; Amy, G.; Minear, R. Applications of Ozone Decomposition Models. *Ozone Sci. Eng.* **1997**, *19*, 5573.

(57) Sehested, K; Holcman, J.; Hart, E. Rate Constants and Products of the Reactions of e_{aq}^-, O_2^-, and H with Ozone in Aqueous Solutions. *J. Phys. Chem.* **1983**, *87*, 1951.

(58) Bühler, R.; Staehelin, J.; Hoigné, J. Ozone Decomposition in Water Studied by Pulse Radiolysis. 1. HO_2/O_2^- and HO_3/O_3^- as Intermediates. *J. Phys. Chem.* **1984**, *88*, 2560.

(59) Sehested, K.; Holcman, J.; Bjergbakke, E.; Hart, E. A Pulse Radiolytic Study of the Reaction $OH+O_3$ in Aqueous Medium. *J. Phys. Chem.* **1984**, *88*, 4144.

(60) Staehelin, R.; Bühler, R.; Hoigné, J. Ozone Decomposition in Water Studied by Pulse Radiolysis. 2. OH and HO_4 as Chain Intermediates. *J. Phys. Chem.* **1984**, *88*, 5999.

(61) Christensen, H.; Sehested, K.; Corfitzen, H. Reactions of Hydroxyl Radicals with Hydrogen Peroxide at Ambient and Elevated Temperatures. *J. Phys. Chem.* **1982**, *86*, 1588.

(62) Buxton, G.; Greenstock, C.; Phyllip, H.; Ross, A. Critical Review of Rate Constants for Reactions of Hydrated Electrons, Hydrogen Atoms and Hydroxyl Radicals ($\cdot OH/\cdot O^-$) in Aqueous Solution. *J. Phys. Chem. Ref. Data* **1988**, *17*, 513.

(63) Bielski, B.; Allen, A. Mechanisms of Disproportionation of Superoxide Radicals. *J. Phys. Chem.* **1977**, *81*, 1048.

(64) Gurol, M.; Akata, A. Kinetics of Ozone Photolysis in Aqueous Solution. *AIChE J.* **1996**, *42*, 3283.

(65) Baxendale, J.; Wilson, J. The Photolysis of Hydrogen Peroxide at High Light Intensities. *Trans. Faraday Soc.* **1956**, *53*, 344.

(66) Oller, I.; Malato, S.; Sánchez-Pérez, J. A. Combination of Advanced Oxidation Processes and Biological Treatments for Wastewater Decontamination - A Review. *Sci. Total Environ.* **2011**, *409*, 4141.

Tables

Table 1. Chemical species that are present in the decomposition of 2,4-D

Measured in this work	
Chemical Species	**Selected references**
2,4-D, ozone, t-BuOH, 2,4-DCP, 2-CHQ, glycolic acid, oxalic acid	5, 7, 12, 20-21, 24, 26, 28, 30, 38, 44-48
Detected traces and ulterior characterization by mass spectroscopy	
Chemical Species	**Selected references**
4,6-dichlororesorcinol, 3,5-dichlorocatechol, maleic acid, fumaric acid, 2,3-dihydroxysuccinic acid, tartaric acid, propanedioic acid, 2-dydroxypropan-edioic acid	12, 28, 30, 39, 44-45, 48-49
Detected by other authors	
Chemical species	**Selected references**
2,4-Dichlororesorcinol, 2- chlorobenzoquinone, 4-chlo-rocatechol, hydroquinone, 2-chloro-4-hydro-xyphenoxyacetic acid, 4-chloro-2-hydroxyphe-noxyacetic acid, glyoxylic acid, 3-hydroxy-2,4-Dichlorophenoxyacetic acid, 5-hydroxy-2,4-Dichloro-phenoxyacetic acid, 6-hydroxy-2,4-Dichlorophenoxyacetic acid. formic acid, acetic acid, glycerol, maleic anhydride, lactic acid, pyruvic acid	5, 12, 21, 28, 30, 38, 44-45, 48-49

Table 2. Reaction mechanism for ozone decomposition in the presence of t-BuOH

Step	Reaction	Kinetic constant – units	Reference
(1)	$O_3 + OH^- \rightarrow HO_2^- + O_2$	$k_1 = 1.7 \times 10^5$ cm^3 mol^{-1} s^{-1}	54
(2)	$O_3 + HO_2^- \rightarrow HO_2^\bullet + O_3^{\bullet-}$	$k_2 = 2.2 \times 10^9$ cm^3 mol^{-1} s^{-1}	55
(3)	$HO_2^\bullet \rightarrow O_2^{\bullet-} + H^+$	$k_3 = 7.9 \times 10^5$ s^{-1}	56
(4)	$O_2^{\bullet-} + H^+ \rightarrow HO_2^\bullet$	$k_4 = 5 \times 10^{13}$ cm^3 mol^{-1} s^{-1}	56
(5)	$O_3 + O_2^{\bullet-} \rightarrow O_3^{\bullet-} + O_2$	$k_5 = (1.6 \pm 0.2) \times 10^{12}$ cm^3 mol^{-1} s^{-1}	57
(6)	$O_3^{\bullet-} + H^+ \rightarrow HO_3^\bullet$	$k_6 = 5 \times 10^{13}$ cm^3 mol^{-1} s^{-1}	58
(7)	$HO_3^\bullet \rightarrow O_3^{\bullet-} + H^+$	$k_7 = 3.3 \times 10^2$ s^{-1}	58
(8)	$HO_3^\bullet \rightarrow {}^\bullet OH + O_2$	$k_8 = 1.1 \times 10^5$ cm^3 mol^{-1} s^{-1}	58
(9)	$O_3 + {}^\bullet OH \rightarrow HO_2^\bullet + O_2$	$k_9 = 1.1 \times 10^{11}$ cm^3 mol^{-1} s^{-1}	59
(10)	$O_2^{\bullet-} + {}^\bullet OH \rightarrow OH^- + O_2$	$k_{10} = (2.8 \pm 0.3) \times 10^7$ cm^3 mol^{-1} s^{-1}	60
(11)	$HO_2^- + H^+ \rightarrow H_2O_2$	$k_{11} = 5 \times 10^{13}$ cm^3 mol^{-1} s^{-1}	56
(12)	$H_2O_2 \rightarrow HO_2^- + H^+$	$k_{12} = 0.125$ s^{-1}	56
(13)	$HO_2^\bullet + {}^\bullet OH \rightarrow H_2O + O_2$	$k_{13} = 5 \times 10^{12}$ cm^3 mol^{-1} s^{-1}	60
(14)	$^\bullet OH + HO_3^\bullet \rightarrow H_2O_2 + O_2$	$k_{14} = 5 \times 10^{12}$ cm^3 mol^{-1} s^{-1}	60
(15)	$^\bullet OH + H_2O_2 \rightarrow HO_2^\bullet + H_2O$	$k_{15} = 2.7 \times 10^{10}$ cm^3 mol^{-1} s^{-1}	61
(16)	$^\bullet OH + HO_2^- \rightarrow HO_2^\bullet + OH^-$	$k_{16} = 7.5 \times 10^{12}$ cm^3 mol^{-1} s^{-1}	61
(17)	$^\bullet OH + {}^\bullet OH \rightarrow H_2O_2$	$k_{17} = 5.2 \times 10^{12}$ cm^3 mol^{-1} s^{-1}	62
(18)	$HO_2^\bullet + HO_2^\bullet \rightarrow H_2O_2 + O_2$	$k_{18} = 8.3 \times 10^8$ cm^3 mol^{-1} s^{-1}	63
(19)	$\text{t-BuOH} + O_3 \rightarrow \text{Prod}_{\text{t-BuOH,1}}$	$k_{19} = 3 \times 10^2$ cm^3 mol^{-1} s^{-1}	39
(20)	$\text{t-BuOH} + {}^\bullet OH \rightarrow \text{Prod}_{\text{t-BuOH,2}}$	$k_{20} = 5 \times 10^{11}$ cm^3 mol^{-1} s^{-1}	39

Table 3. Concentration of •OH radicals in the presence of t-BuOH

Time	•OH **Conc. (mol cm^{-3})**
0 s	1×10^{-15} (a)
20 s	1.4×10^{-14} (b)
3 min.	1×10^{-20}
15 min.	1×10^{-25}
40 min.	1×10^{-30}
70 min.	1×10^{-35}
90 min.	1×10^{-40}
120 min.	1×10^{-45}
140 min.	1×10^{-50}

(a): Initializing concentration. (Taken from Westerhoff et al.[56]).
(b): Maximum value.

Table 4. Kinetic constants to complete the reaction scheme.

Step	Reaction	Kinetic Constant - units	Ref.
(21)	$2,4-D + O_3 \rightarrow 2,4-DCP + Prod_4$	$k_{21} = (1.00 \pm 0.09) \times 10^3$ cm^3 mol^{-1} s^{-1}	i
(22)	$2,4-DCP + O_3 \rightarrow 2-CHQ + Prod_5$	$k_{22} = (1.22 \pm 0.06) \times 10^4$ cm^3 mol^{-1} s^{-1}	ii
(23)	$2-CHQ + O_3 \rightarrow Prod_6$	$k_{23} = (3.37 \pm 0.02) \times 10^4$ cm^3 mol^{-1} s^{-1}	iii
(24)	$2,4-D + {}^{\bullet}OH \rightarrow 2,4-DCP + Prod_7$	$k_{24} = (4.00 \pm 0.23) \times 10^{11}$ cm^3 mol^{-1} s^{-1}	iv
(25)	$2,4-DCP + {}^{\bullet}OH \rightarrow 2-CHQ + Prod_8$	$k_{25} = (7.58 \pm 0.59) \times 10^{12}$ cm^3 mol^{-1} s^{-1}	v
(26)	$2-CHQ + {}^{\bullet}OH \rightarrow Prod_9$	$k_{26} = (8.12 \pm 0.76) \times 10^{12}$ cm^3 mol^{-1} s^{-1}	vi
(27)	$2,4-D \xrightarrow{h\nu} 2,4-DCP + Prod_1$	$\phi_{2,4-D}$ =0.016 mol Einstein^{-1}	vii
(28)	$2,4-DCP \xrightarrow{h\nu} 2-CHQ + Prod_2$	$\phi_{2,4-DCP}$ = 0.017 mol Einstein^{-1}	viii
(29)	$2-CHQ \xrightarrow{h\nu} Prod_3$	ϕ_{2-CHQ} = 0.041 mol Einstein^{-1}	ix
(30)	$O_3 + H_2O \xrightarrow{h\nu} H_2O_2 + O_2$	ϕ_{O_3} = 0.50 mol Einstein^{-1}	64
(31)	$H_2O_2 \xrightarrow{h\nu} 2\ {}^{\bullet}OH$	$\phi_{H_2O_2}$ = 0.48 mol Einstein^{-1}	65

i, ii, iii, iv, v, vi, vii, viii and ix: this work.

Figures

Figure 1

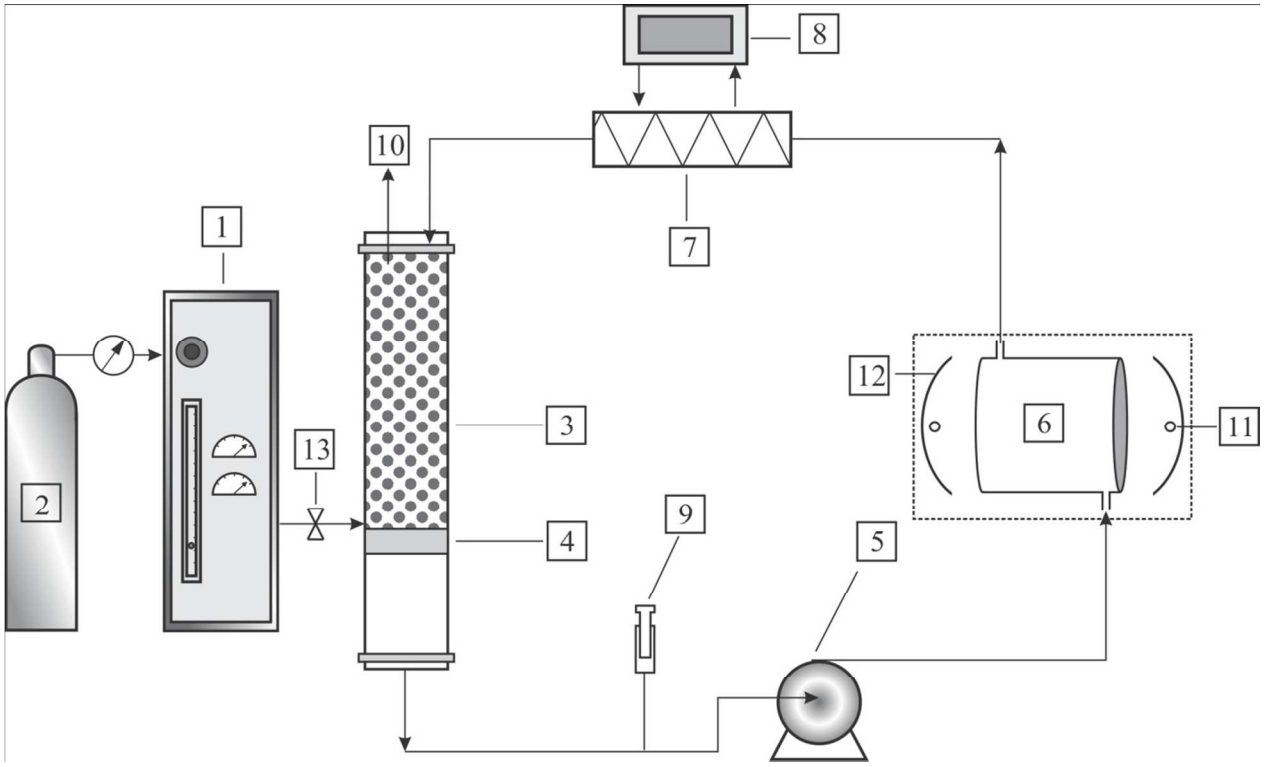

Figure 2

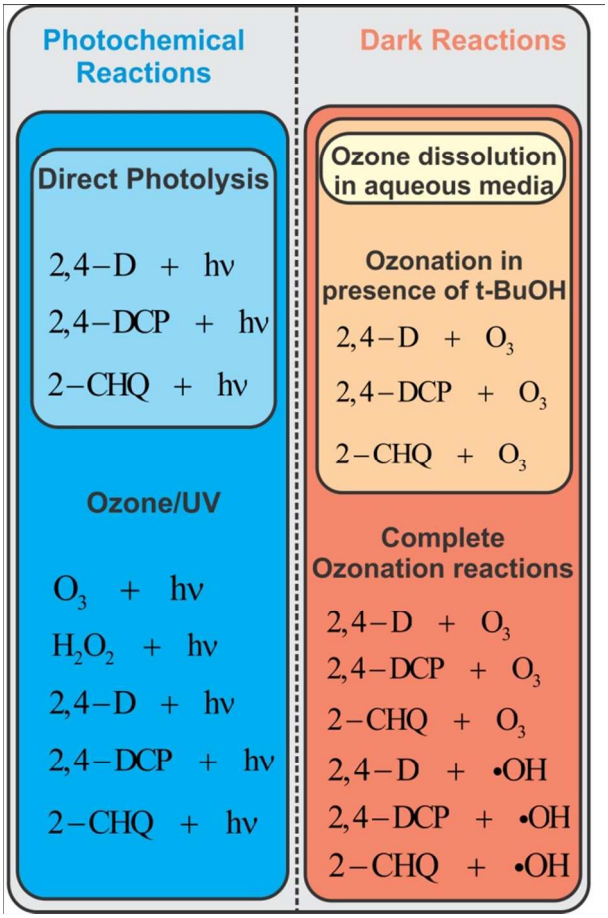
Photochemical Reactions
Dark Reactions
Direct Photolysis
2,4−D + hν
2,4−DCP + hν
2−CHQ + hν
Ozone/UV
O3 + hν
H2O2 + hν
2,4−D + hν
2,4−DCP + hν
2−CHQ + hν
Ozone dissolution in aqueous media
Ozonation in presence of t-BuOH
2,4−D + O3
2,4−DCP + O3
2−CHQ + O3
Complete Ozonation reactions
2,4−D + O3
2,4−DCP + O3
2−CHQ + O3
2,4−D + •OH
2,4−DCP + •OH
2−CHQ + •OH

Figure 3

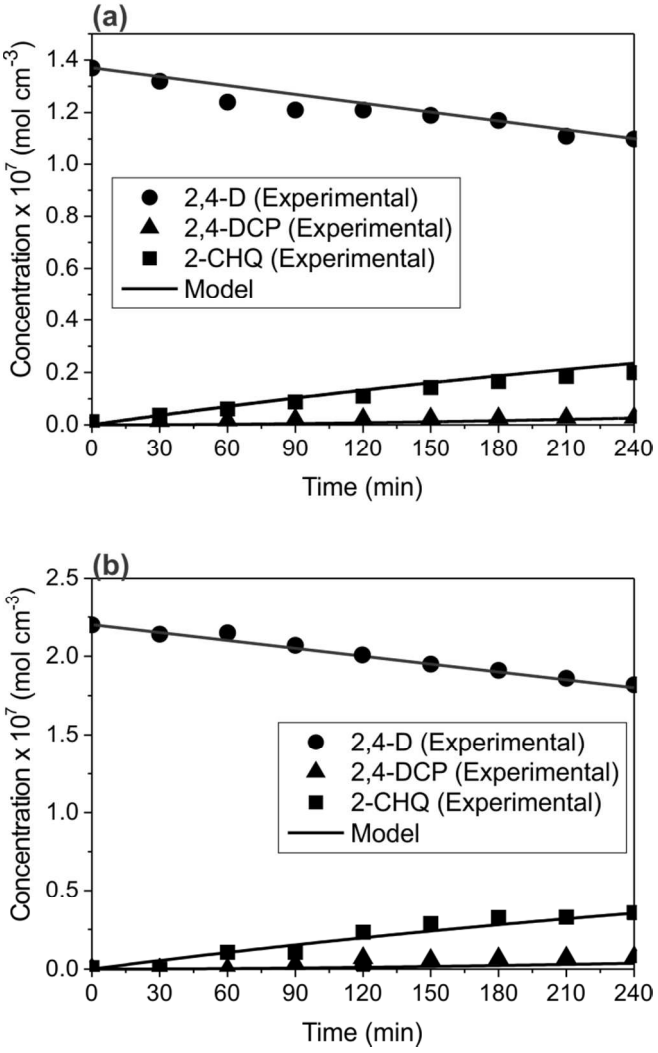
(a)
Concentration x 10^7 (mol cm^-3)
1.4
1.2
1.0
0.8
0.6
0.4
0.2
0.0
0
30
60
90
120
150
180
210
240
Time (min)
2,4-D (Experimental)
2,4-DCP (Experimental)
2-CHQ (Experimental)
Model
(b)
Concentration x 10^7 (mol cm^-3)
2.5
2.0
1.5
1.0
0.5
0.0
0
30
60
90
120
150
180
210
240
Time (min)
2,4-D (Experimental)
2,4-DCP (Experimental)
2-CHQ (Experimental)
Model

Figure 4

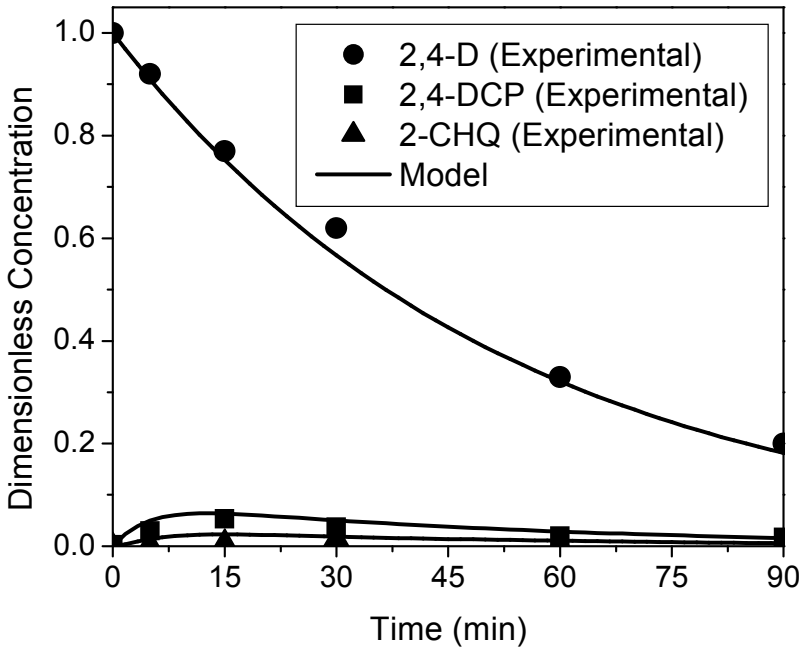
2,4-D (Experimental)
2,4-DCP (Experimental)
2-CHQ (Experimental)
Model
Dimensionless Concentration
Time (min)
0.0
0.2
0.4
0.6
0.8
1.0
0
15
30
45
60
75
90

Figure 5

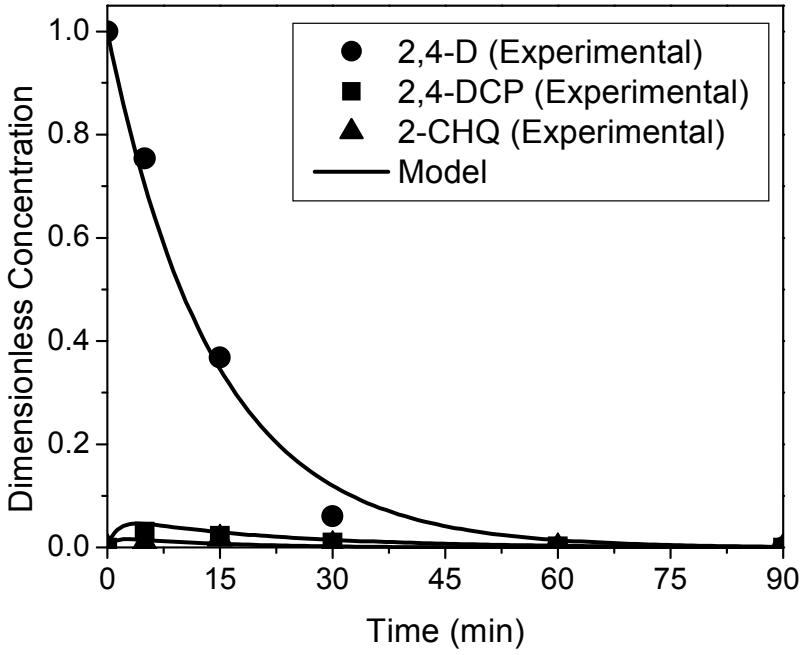
2,4-D (Experimental)
2,4-DCP (Experimental)
2-CHQ (Experimental)
Model
Dimensionless Concentration
Time (min)
0.0
0.2
0.4
0.6
0.8
1.0
0
15
30
45
60
75
90

Figure 6

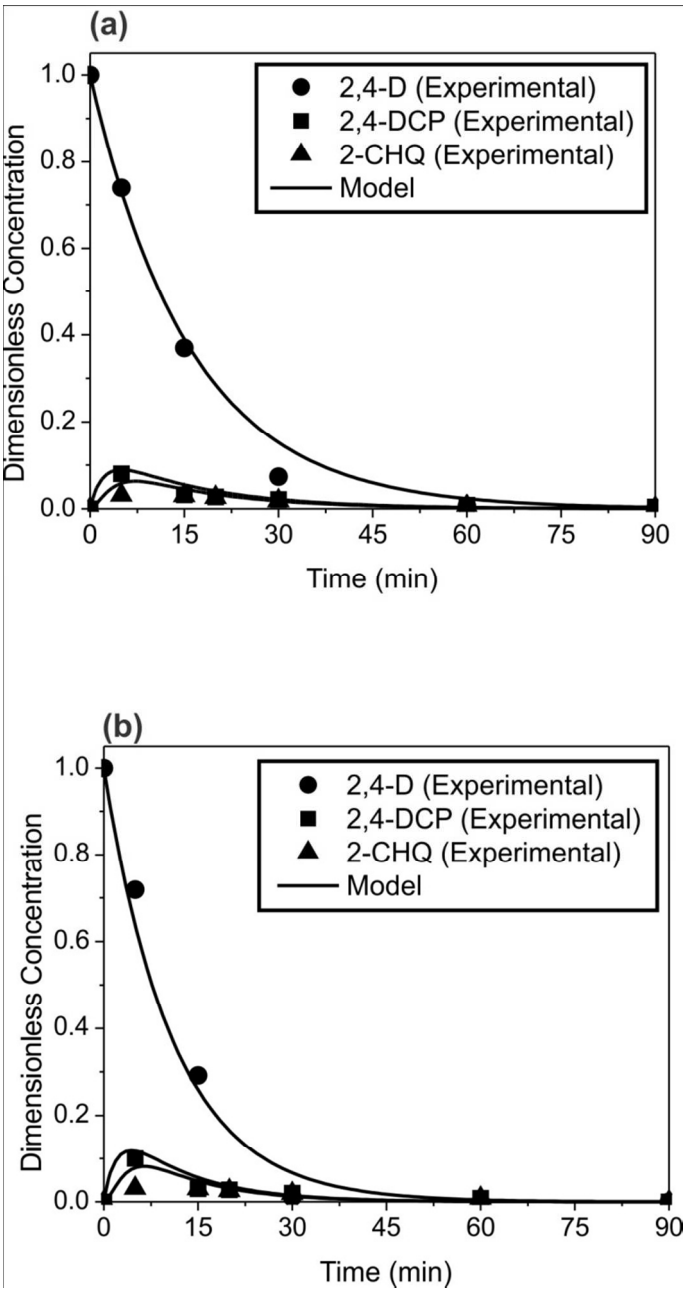
(a)
2,4-D (Experimental)
2,4-DCP (Experimental)
2-CHQ (Experimental)
Model
Dimensionless Concentration
Time (min)
(b)
2,4-D (Experimental)
2,4-DCP (Experimental)
2-CHQ (Experimental)
Model
Dimensionless Concentration
Time (min)

Figure 7

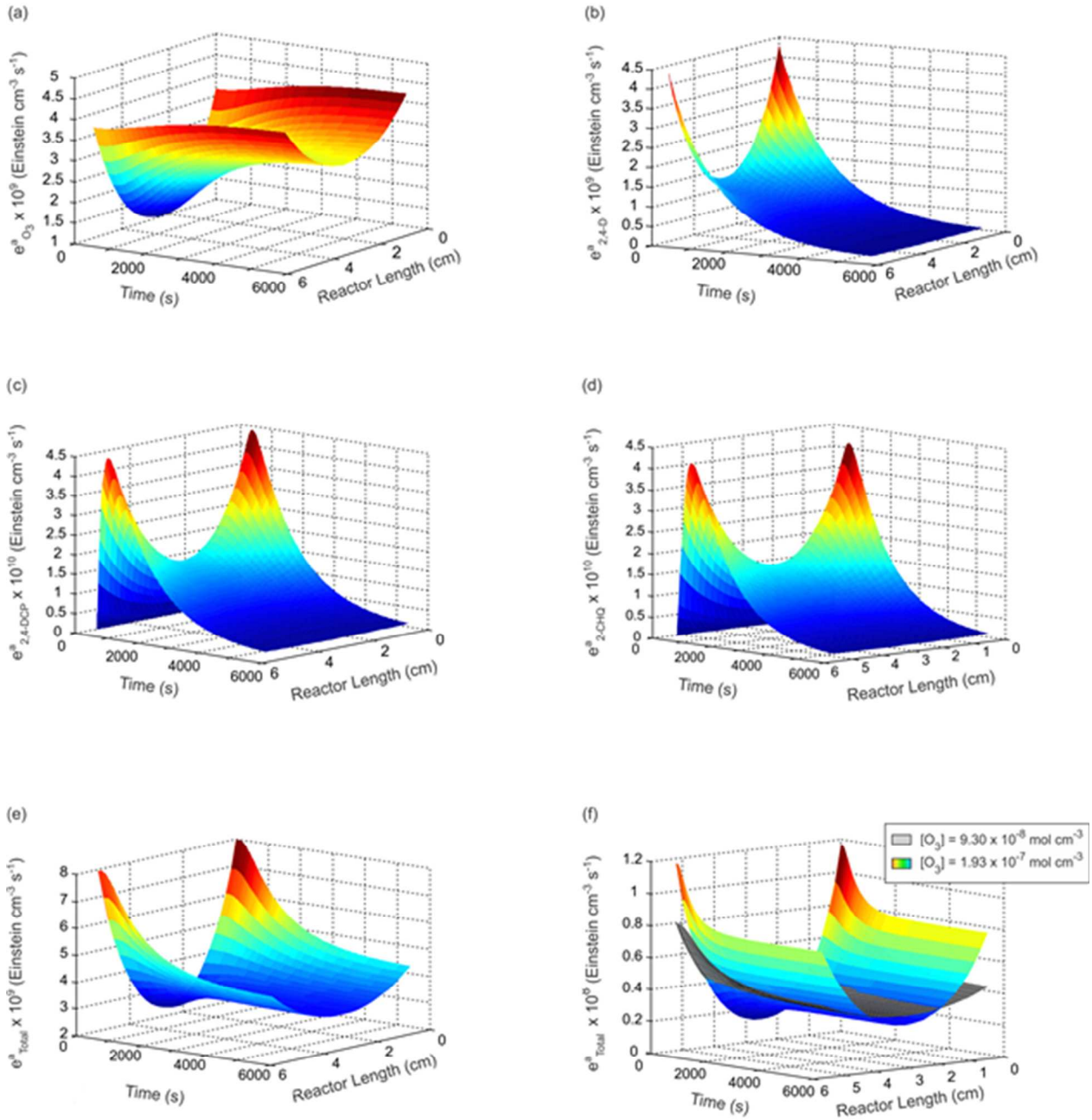
(a)
$e^a_{O_3}$ x 10^9 (Einstein cm^{-3} s^{-1})
Time (s)
Reactor Length (cm)
(b)
$e^a_{2,4\text{-}D}$ x 10^9 (Einstein cm^{-3} s^{-1})
Time (s)
Reactor Length (cm)
(c)
$e^a_{2,4\text{-}DCP}$ x 10^{10} (Einstein cm^{-3} s^{-1})
Time (s)
Reactor Length (cm)
(d)
$e^a_{2\text{-}CHO}$ x 10^{10} (Einstein cm^{-3} s^{-1})
Time (s)
Reactor Length (cm)
(e)
e^a_{Total} x 10^9 (Einstein cm^{-3} s^{-1})
Time (s)
Reactor Length (cm)
(f)
e^a_{Total} x 10^5 (Einstein cm^{-3} s^{-1})
$[O_3]$ = 9.30 x 10^{-8} mol cm^{-3}
$[O_3]$ = 1.93 x 10^{-7} mol cm^{-3}
Time (s)
Reactor Length (cm)

Figure 8

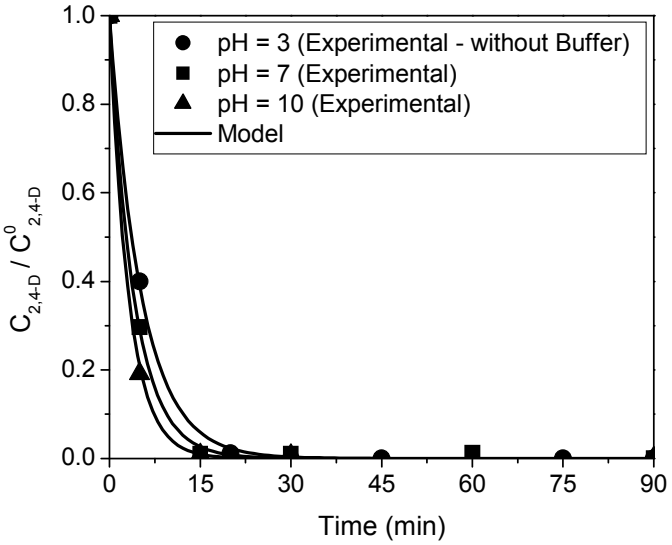
pH = 3 (Experimental - without Buffer)
pH = 7 (Experimental)
pH = 10 (Experimental)
Model
$C_{2,4\text{-D}} / C^0_{2,4\text{-D}}$
Time (min)
0.0
0.2
0.4
0.6
0.8
1.0
0
15
30
45
60
75
90

Figure 9

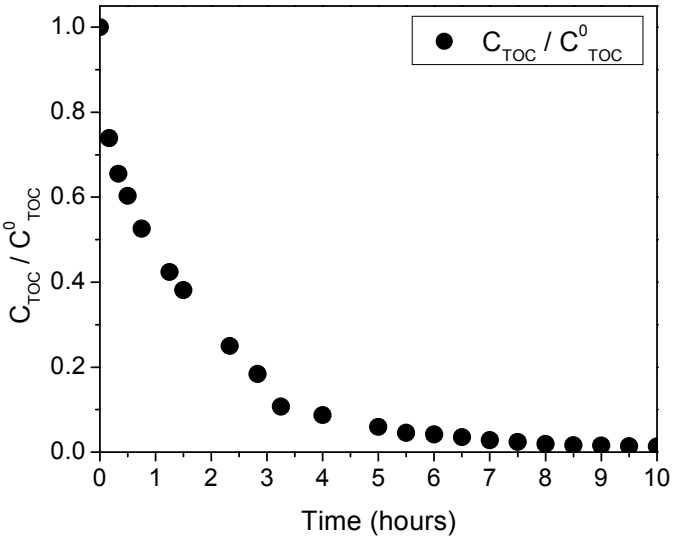
1.0
0.8
0.6
0.4
0.2
0.0
0
1
2
3
4
5
6
7
8
9
10
Time (hours)
C_TOC / C^0_TOC
C_TOC / C^0_TOC

Figure 10

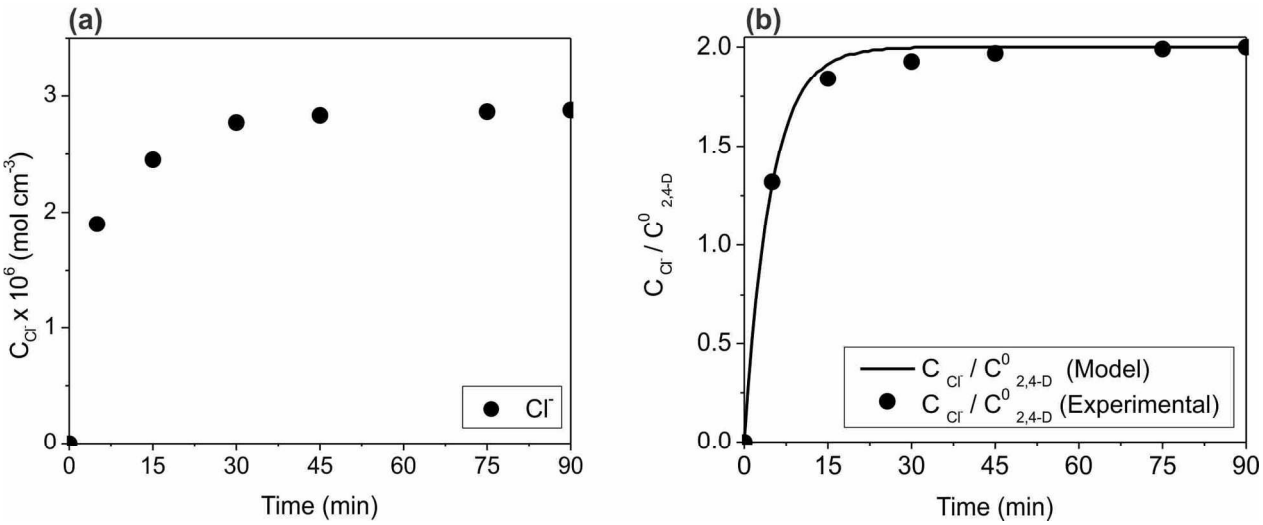
(a)
C_{Cl^-} x 10^6 (mol cm^{-3})
Time (min)
Cl^-
(b)
$C_{Cl^-} / C^0_{2,4\text{-}D}$
Time (min)
$C_{Cl^-} / C^0_{2,4\text{-}D}$ (Model)
$C_{Cl^-} / C^0_{2,4\text{-}D}$ (Experimental)

Figure captions

Figure 1. Reactor configuration. (1) Ozone generator. (2) O_2 cylinder. (3) Absorption column. (4) Perforated plate. (5) Centrifugal pump. (6) Photoreactor. (7) Heat exchanger. (8) Thermostatic bath. (9) Sampling port. (10) Venting outlet. (11) Germicidal lamps. (12) Parabolic reflectors. (13) Intake valve

Figure 2. Conceptual reaction scheme

Figure 3. Direct photolysis. (a) $C^0_{2,4-D}$=1.37 × 10^{-7} mol cm^{-3} (30 ppm) and (b) $C^0_{2,4-D}$=2.20 × 10^{-7} mol cm^{-3} (50 ppm). Symbols correspond to experimental data. Solid lines correspond to simulation results obtained from the model.

Figure 4. Direct reaction with molecular ozone. Comparison of simulation predictions with experimental data. $C_{O_3} = 3.18 \times 10^{-7}$ mol cm^{-3}

Figure 5. Reaction with ozone in the absence of t-BuOH. Comparison of simulation predictions with experimental data. $C_{O_3} = 3.01 \times 10^{-7}$ mol cm^{-3}.

Figure 6. Results of the complete kinetic sequence. $C_{O_3} = 1.21 \times 10^{-7}$ mol cm^{-3}. (a) Lamp: Nominal input power = 15W. (b) Lamp: Nominal input power = 40W.

Figure 7. LVRPA as a function of time and reactor length: (a) ozone, (b) 2,4-D, (c) 2,4-DCP and (d) 2-CHQ; (e) Total local volumetric rate of photon absorption. $C_{O_3} = 1.93 \times 10^{-7}$ mol cm^{-3} for all these figures; (f) Effect of different ozone concentration, $C_{O_3} = 9.30 \times 10^{-8}$ mol cm^{-3} and 1.93 × 10^{-7} mol cm^{-3}. Lamp: 40W in all cases.

Figure 8. Effect of modification of the pH. Ozone concentration=2.9 ×10^{-7} mol cm^{-3}.
Lamps: Nominal input power=40W in all cases. Data at pH 7 and 10, employing buffer solutions

Figure 9. TOC reduction.

Figure 10. (a) Chloride ion concentration and (b) Ratio of chloride ion formation with respect to 2,4-D decomposition: experimental and theoretical results.

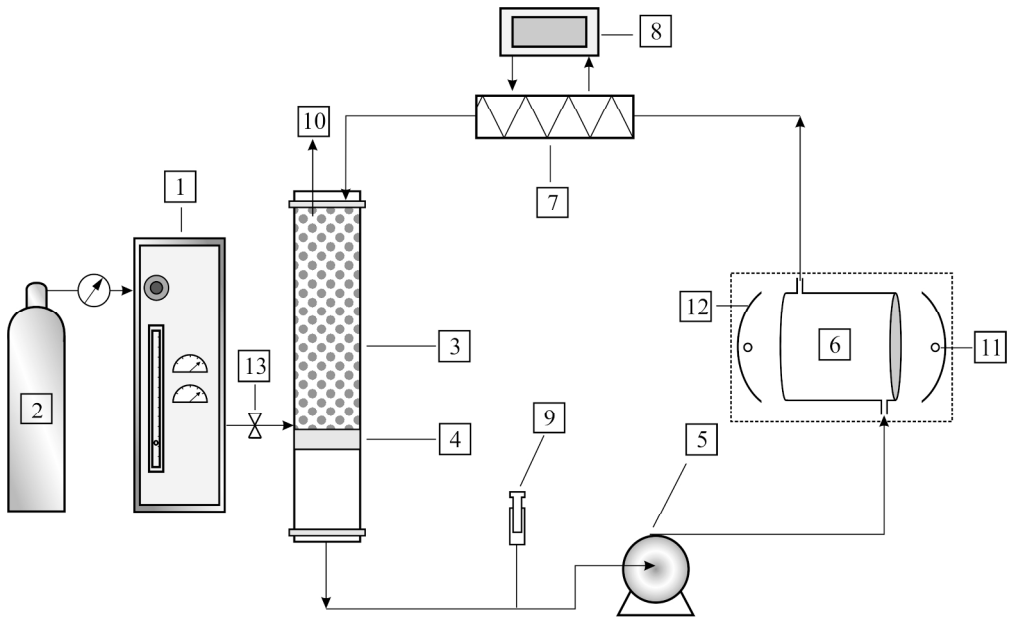

208x126mm (300 x 300 DPI)

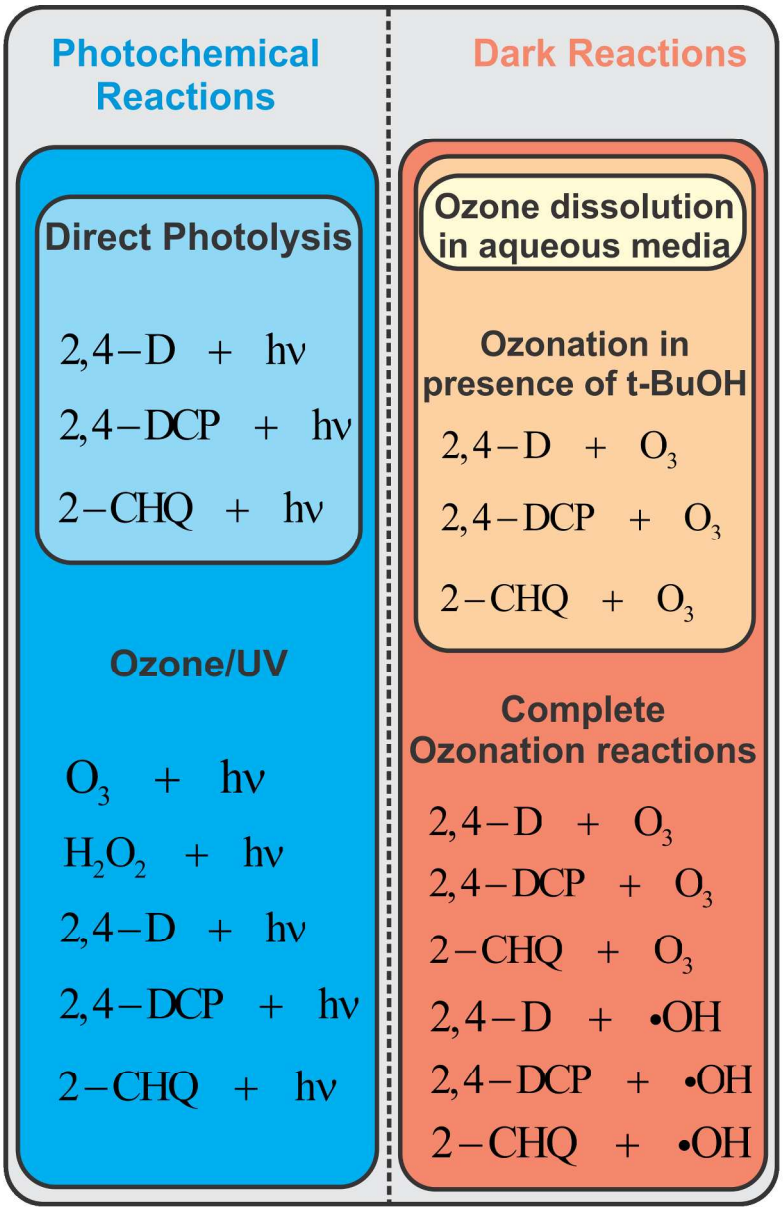

178x269mm (300 x 300 DPI)

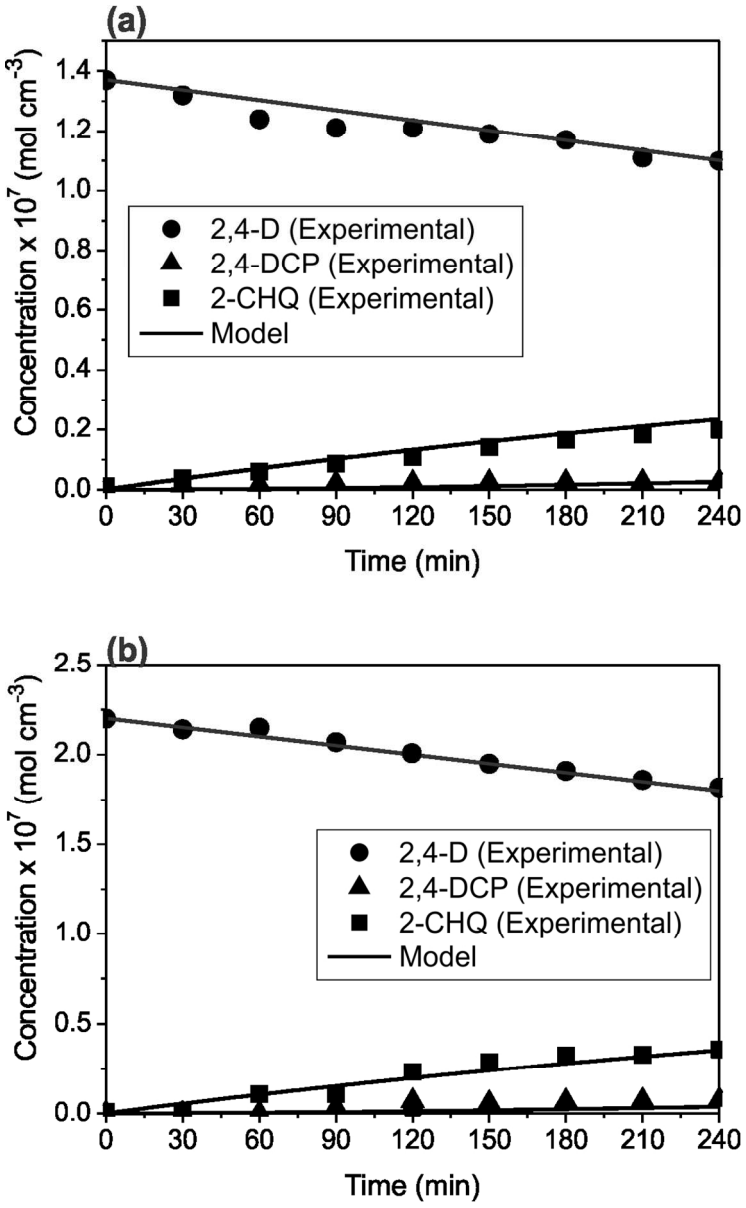

94x153mm (300 x 300 DPI)

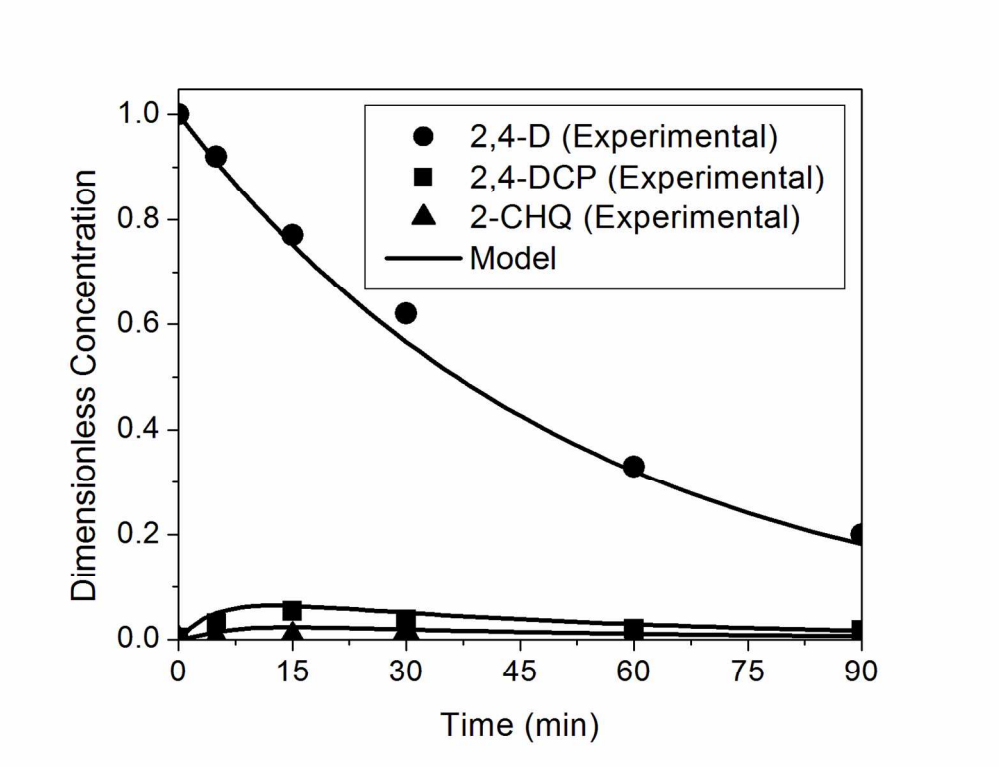

273x209mm (150 x 150 DPI)

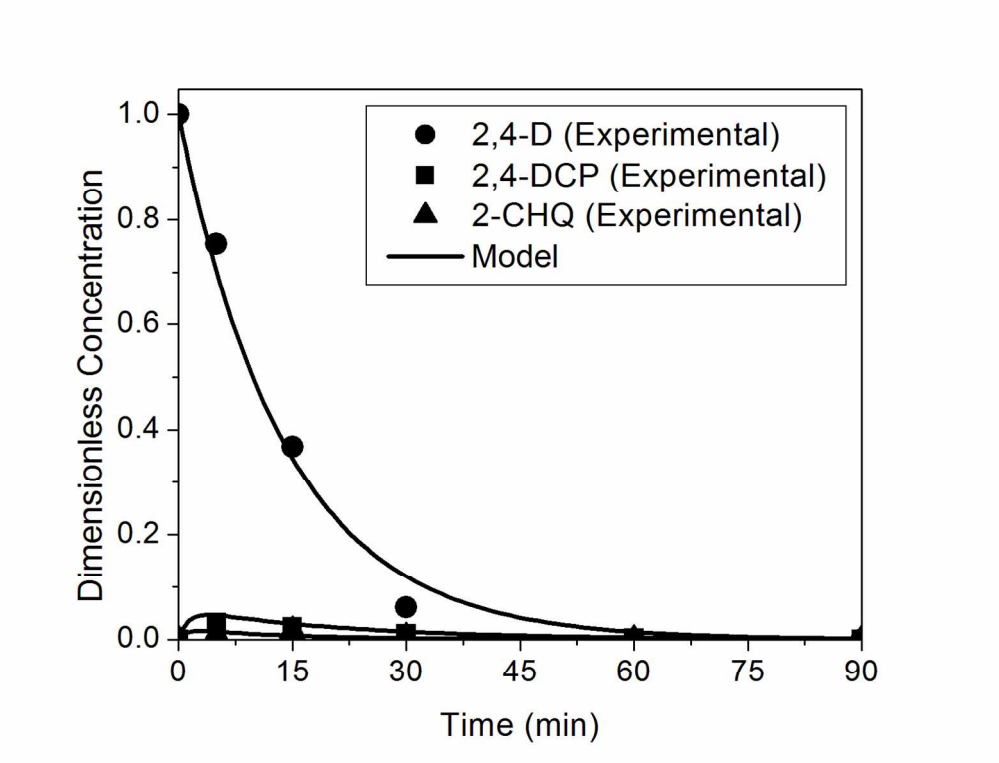

273x209mm (150 x 150 DPI)

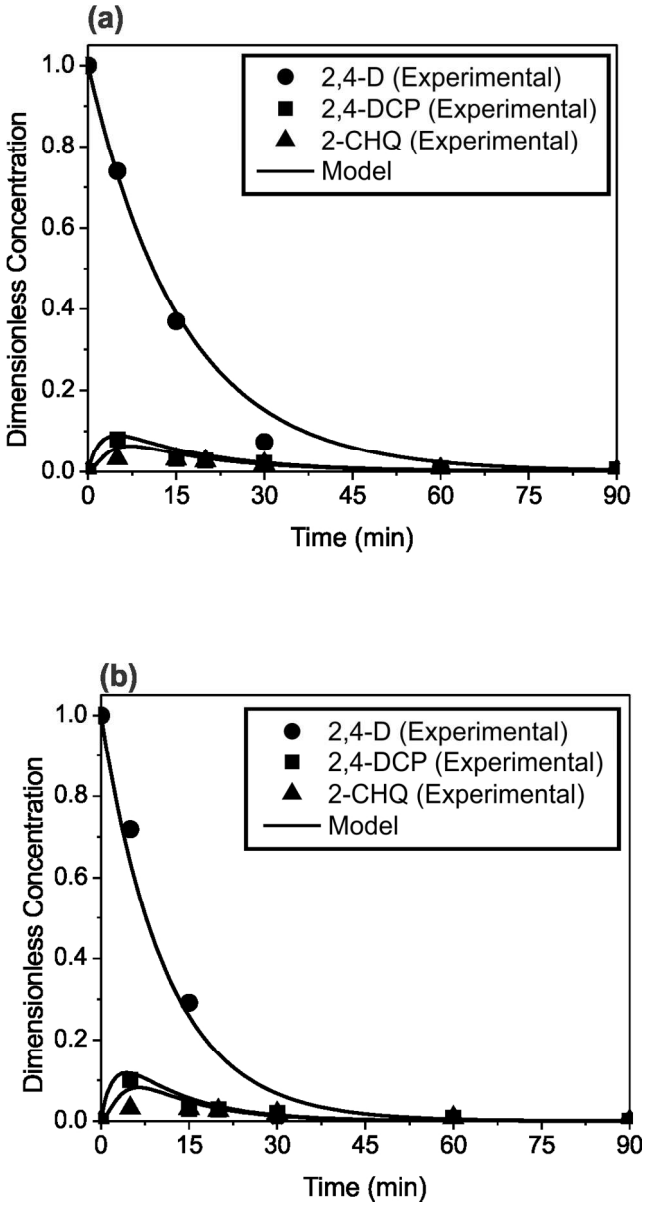

89x169mm (300 x 300 DPI)

Unable to Convert Image

The dimensions of this image (in pixels) are too large to be converted. For this image to convert, the total number of pixels (height x width) must be less than 40,000,000 (40 megapixels).

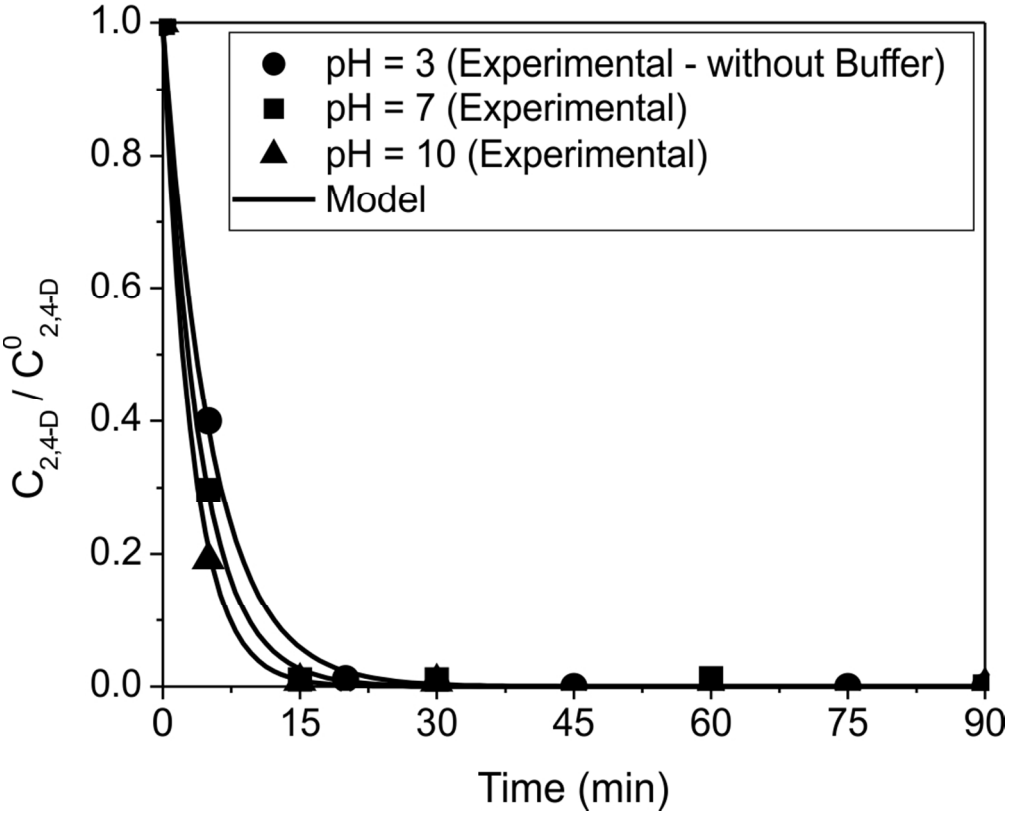

90x74mm (300 x 300 DPI)

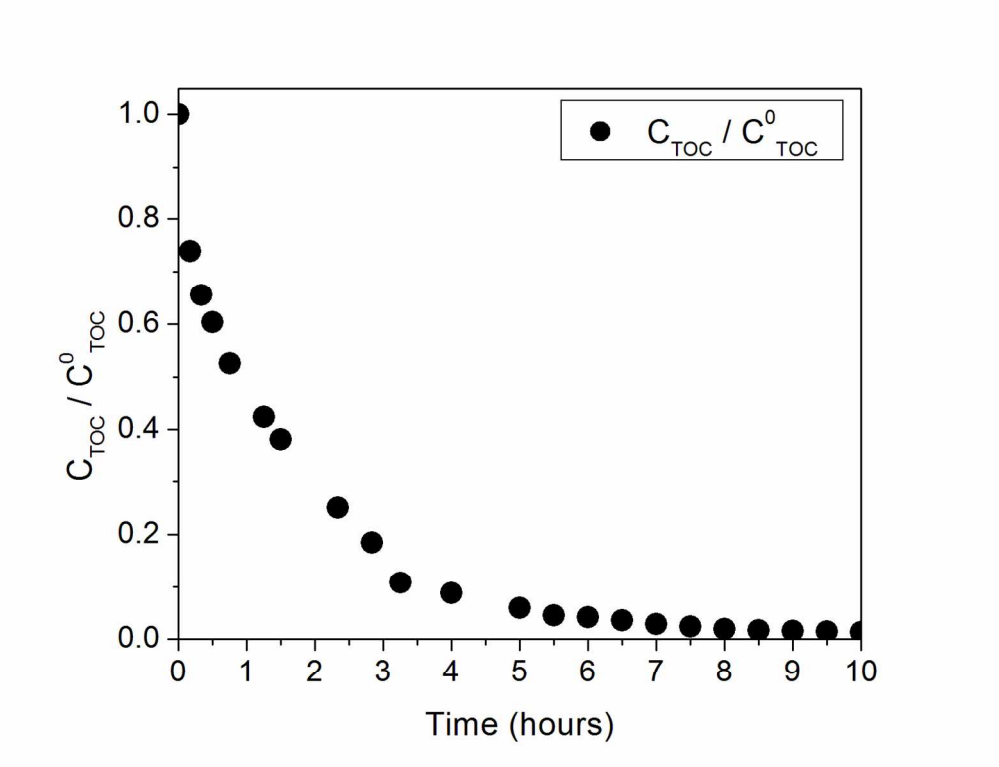

273x209mm (150 x 150 DPI)

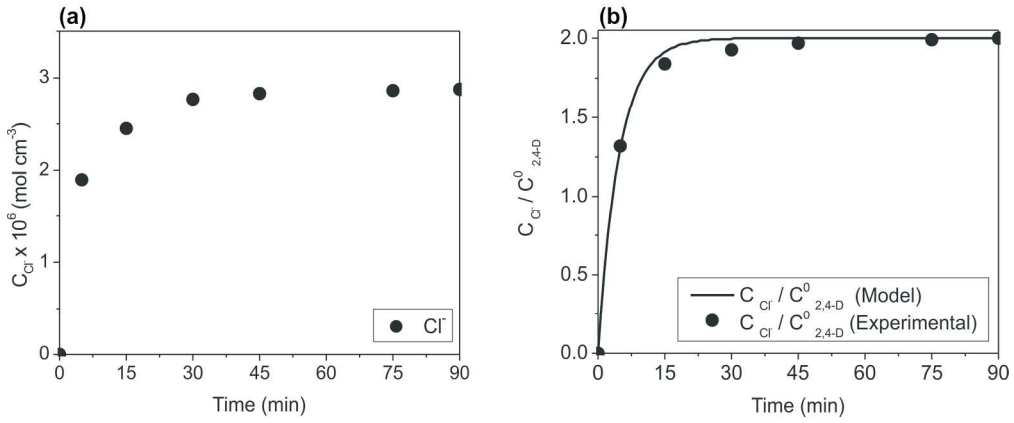

186x76mm (300 x 300 DPI)